Robust real-time economic optimization and parameter estimation of post-combustion CO_2 capture under economic uncertainty

Gabriel D. Patrón[a], Luis Ricardez-Sandoval[a]*

[a]Department of Chemical Engineering, University of Waterloo, Waterloo, ON, Canada N2L 3G1

Abstract

The operational cost of post-combustion carbon capture remains the principal factor impeding its uptake, thus real-time optimization has been proposed for economic operation. This requires that uncertainties be estimated, subjecting its solutions to estimation error. Herein, we propose uncertainty estimation and real-time optimization for post-combustion carbon capture plants. Model parameters are estimated using noisy measurements to address model uncertainty; accordingly, we deploy a low-variance scheme to address noise propagation. Our approach is implemented in a pilot-scale carbon capture plant through uncertain flue gas compositions and thermodynamic activities. The proposed method results in operating points closer to the true optima, with up to 25% improvement in economics compared to alternative operational approaches. Moreover, a robust real-time optimization strategy is proposed for cases in which model parameters and economic factors are simultaneously uncertain. The robust update strategy is deployed jointly with the low-variance estimation scheme to quantify the uncertainty in each model parameter, resulting in economic improvements and a notable reduction (~80%) in the set point variability over the standard update approach. Through the schemes proposed, the carbon capture plant was able to operate at set points with high capture rates, low energy consumption, and low cost. This suggests that the proposed approach is suitable for the economic optimization of other energy and carbon capture systems.

Keywords: Post-combustion carbon capture, Real-time optimization, Parameter estimation

*Corresponding author: e-mail: laricard@uwaterloo.ca, phone: (+1) 519 888 4567 x38667, fax, (+1) 519 888 4347

1. Introduction

While the worldwide demand for sustainable systems grows, greenhouse gas (GHG) emissions remain deeply entrenched with the methods used to produce energy. CO_2 is the most abundant of the GHGs and makes the greatest contribution to global warming, accounting for an increase of ~0.75℃ in the last decade relative to the late 19th century (Masson-Delmotte et al., 2021). The production of CO_2 is particularly sizable in large and developing economies (IEA, 2021), which require fossil fuels to meet growing energy demands. Many mitigation strategies have been proposed to abate the production of CO_2; chiefly among these is carbon capture and storage (CCS), which aims to remove and sequester CO_2 from industrial sources for later repurposing or deposition in reservoirs.

CCS can be achieved through several methods including adsorption (Ben-Mansour et al., 2016), chemical looping combustion (Lucio and Ricardez-Sandoval, 2020), membrane gas separation (Khalilpour et al., 2016), oxy-fuel combustion (Chansomwong et al., 2014), and post-combustion capture (PCC) (Chao et al., 2021; Gaspar et al., 2016; Liu et al., 2019). Of these technologies, PCC is the most developed, with pilot-scale (Dugas, 2006; Tontiwachwuthikul et al., 2022) and industrial-scale (Huang et al., 2010; Monañés et al., 2018) plants in operation. Despite the maturity of PCC, its widespread adoption in industry has been slow. This is primarily owed to the PCC process economics, which, under the current incentives, pose a net financial detriment to the associated upstream power plant where profit is prioritized.

To overcome the issue of prohibitive cost, extensive analyses have been conducted on the economics of PCC plants under varying operational modes and assumptions (e.g., different upstream processes, power plant fuels and loads, and carbon tax rates) (Carminati et al., 2019; Danaci et al., 2021; Jiang et al., 2021; Nwaoha and Tontiwachwuthikul, 2021). Other approaches have looked to find economical operational schemes for PCC (Luu et al., 2015; Mechleri et al., 2017; Panahi et al., 2012), including various optimization schemes at different timescales. Nonetheless, many of these approaches consider constant carbon capture rates, which are maintained by a control layer. In contrast, while less investigated in the PCC literature, some authors have proposed using model-based optimization to update the process in real time; these allow for frequent updating of the PCC operation to match changing upstream power plant and process conditions. Real-time production schemes, which typically use high-fidelity models, can be divided into two broad categories: economic model predictive control (EMPC; Ellis et al., 2014) and real-time optimization (RTO; Darby et al., 2011).

EMPC uses a dynamic optimization approach to determine economically optimal actions for plant manipulated variables, while RTO uses steady-state optimization to update process set points to be tracked by a controller. Chan and Chen (2018) and Decardi-Nelson et al. (2018) have both applied an EMPC approach for the operation of PCC. The former considered solvents and utility costs while the latter considered carbon taxes and energy costs. Recently, Decardi-Nelson and Liu (2022) proposed a robust EMPC that considered absorber efficiency while accounting for model uncertainty and disturbances using a zone modification method. For RTO, Decardi-Nelson et al. (2018) proposed a scheme with an equivalent objective function to their EMPC scheme, while Akula et al. (2021) considered pumping, cooling, and heating costs in an alternative RTO formulation. Despite the variety of proposed real-time economic optimization schemes in the PCC literature, all the previous approaches omitted significant aspects of PCC economics, thus limiting their real-life application. Our previous works (Patrón and Ricardez-Sandoval, 2020a; 2022a) filled this gap by introducing the most comprehensive PCC economic function posed in a generic way as to be applied to any PCC plant (e.g., with different designs and solvents). Moreover, we integrated the RTO scheme with a control and state estimation procedure.

Process models used for optimization are subject to idealizations or experimentally determined parameters leading to plant–model mismatch. In energy systems, where the behaviour is often nonlinear and subject to large disturbances and parametric uncertainty, this can result in large deviations between plant outputs and model predictions. Accordingly, energy system models should be continually updated, thereby reconciling the model with the plant which can address uncertainty to achieve near-optimal performance. Uncertainty is particularly salient in PCC where a nonlinear carbon capture plant interacts with a nonlinear power plant. Accordingly, this topic has been investigated for several applications. The design of PCC under uncertainty has been addressed through ranking-based (Bahakim and Ricardez-Sandoval, 2015) and multi-scenario (Cerrillo-Briones and Ricardez-Sandoval, 2019) approaches. In the control layer, several robust controllers (Jung et al., 2020; Rúa et al., 2021; Zhang et al., 2018) have been proposed and paired with various state estimators (Patrón and Ricardez-Sandoval, 2022a; Yin et al., 2020); these often consider uncertain model structures, parameters, and unmeasurable/unmeasured variables. On longer timescales, scheduling (Zantye et al., 2019) and planning (Wu et al., 2015; Xuan et al., 2022; Zhang et al., 2021) schemes have been proposed for PCC, which generally address price and demand uncertainties. As per the literature, uncertainty has only been considered for online economic optimization of PCC in the context of EMPC (Decardi-Nelson and Liu, 2022); however, no study has considered uncertainty in an RTO-operated PCC process. The effect of uncertainty in real-time

steady-state decision making (i.e., not scheduling or planning time horizons) for PCC is unknown. To the authors' knowledge, the online optimization studies for PCC described above limit their operating time to days at most, hence the interactions between decisions made in real-time with long-term process outcomes also remain unknown.

While the models used in RTO are often mechanistic, there is no guarantee that the model parameters are near their true values; hence, parameters estimation schemes must be considered to improve the RTO's predictions. Indeed, for a PCC system being modelled mechanistically, Hughes et al. (2022) recently showed the importance of parameter accuracy through uncertainty quantification of mass transfer and kinetic parameters and their impacts on the effectiveness of carbon capture. To this end, RTO schemes typically employ the so-called 'two-step' approach, whereby a parameter estimation (PE) layer is employed to update RTO model parameters periodically. RTO and PE have been considered independently for many systems including sludge-to-methane (Shi et al., 2022), hydrogen production PE (Xu et al., 2020), and poultry litter utilization (Ma et al., 2022). However, previous RTO implementations for PCC, have not considered the estimation layer of the two-step approach (i.e., they have assumed perfect parameters and measurable disturbances). In most of the cases, this is a strong assumption as online measurement of some disturbances (e.g., compositions) or perfect knowledge of model parameters (e.g., thermodynamic activities or mass transfer parameters) are not realistic. As such, this assumption remains to be addressed such that the PCC RTO is fully implementable in a real-life scenario. In contrast, cases with rapidly fluctuating parameters and economics make the two-step approach for RTO unsuitable as set points can quickly become suboptimal. Instead, a robust optimization approach could be deployed for this task. However, robust optimization, which has been an active research consideration for PCC in longer timescales, has also yet to be considered in context of RTO.

An additional complicating factor to the uncertainty problem in RTO is measurement noise, which is unavoidable because of random fluctuations and instrumentation error. If the measurements are sufficiently noisy, parameter estimates may be computed with high error; this will cause erroneous set points to be produced by the RTO, leading economically suboptimal plant operation. In PCC plants, or indeed any large-scale energy system with many interactions and nonlinearities, the optimal steady-state operating point will be highly sensitive to model inputs such that noisy variations could have large economic and environmental consequences (e.g., increased losses and emissions). Methods to deal with this noise propagation, namely data reconciliation (DR; Bhat and Saraf, 2004; Miletic and Marlin, 1998; Yuan et al., 2015), have been proposed for this purpose. DR generally reconciles noisy

110 measurements with process models such that the measurements are consistent with the model. This approach,
111 however, does not address the individual measurements explicitly because it is not selective of which measurements
112 are used despite potentially varying impacts on the downstream estimation scheme. Moreover, the DR methods in the
113 literature require the application of sensitivity information or additional process layers (e.g., Kalman filter and least-
114 squares minimization), respectively. While sensitivity information is computationally expensive to acquire in practice,
115 the implementation of many additional decision layers is undesirable as it could make an already stratified processing
116 scheme such as RTO increasingly convoluted. This leaves a gap for a practical method to deal with the issue of noise
117 as it pertains to the steady-state estimation problem of process systems. In energy generation and its ancillary processes
118 like PCC, where the process economics are paramount, the improvements made in abating the effects of noise in
119 operating conditions may become a critical factor. Studies addressing the issue of measurement noise and data
120 processing for PCC have not been reported.
121 Based on the above, uncertainty in the real-time optimization of PCC plants has not been explicitly addressed. To the
122 authors' knowledge, noisiness also remains an open issue as it pertains to PCC estimation schemes and no method has
123 been tested to abate its effects in CO_2 capture systems; hence, the effect of parameter fidelity on model-based control
124 and optimization performance for PCC has not been reported. In addition, parameter and economic robustness have
125 not been jointly addressed in the online optimization of PCC. In particular, our previous work (Patrón and Ricardez-
126 Sandoval, 2022a), which is the most comprehensive RTO implementation in PCC to date, did not consider any type
127 of uncertainty and a very limited set of disturbances. Accordingly, a detailed exploration of the optima across possible
128 disturbances ranges, the addition of novel parameter estimation, and robust optimization layers, will provide new
129 insights on the remaining computational challenges (i.e., uncertainty and noise) that could inhibit the deployment of
130 online economic optimization in PCC plants. The specific objectives considered in the present study are as follows:
131 1. A high-fidelity framework is proposed for the estimation of uncertainties in high noise environments without
132 requiring data reconciliation. Model uncertainty in the thermodynamic parameters and flue gas compositions
133 for PCC are estimated in the context of RTO.
134 2. The proposed estimation scheme is compared to our previous work (Patrón and Ricardez-Sandoval, 2022a)
135 and DR via their respective impacts on PCC performance. These analyses are performed on a long (i.e.,
136 month) timescale to assess the impact of real-time decisions on long-term PCC operation.

3. A sensitivity analysis is performed for the optimal cost and rate of carbon capture. The effect of disturbances and economic incentives are quantified for the optimal operation of PCC.
4. A new robust RTO scheme is presented along with an update strategy for PCC set points under diurnal operation. The proposed estimation scheme is also used for uncertainty quantification to yield robust solutions. This new robust RTO scheme explicitly and simultaneously considers uncertainty in the economic parameters and in the model parameters of the CO_2 capture plant.

This work is structured as follows: section 2 details the formulation for the PE scheme and the robust RTO formulation; section 3 briefly overviews PCC and introduces assessment metrics and constraints for the proposed scheme; section 4 exhibits the test scenarios on the proposed scheme; and section 5 summarizes the insights gained from this study and outlines future works. A nomenclature section can be found at the end.

2. Proposed scheme and formulations

RTO is a model-based optimization method that has been proposed in the literature (e.g., Darby et al., 2011) to achieve the economically optimal steady-state operation of process systems. As the models used for RTO are subject to uncertainty, the two-step RTO approach is deployed, which continually updates the model via estimation of parameters. The estimation step, which uses available steady-state process measurements, can address parametric uncertainties in the phenomenological model parameters and external disturbances. In addition to parametric uncertainty, uncertainty also manifests through measurement noise. If the system is noisy, this can adversely impact the fidelity of estimates acquired using the measurements; no practical method or assessment of this issue has been proposed in the context of PCC. This section presents the general formulation for RTO under uncertainty, a noise-abatement scheme to ensure estimates are indeed reliable, and a robust RTO to address price fluctuations.

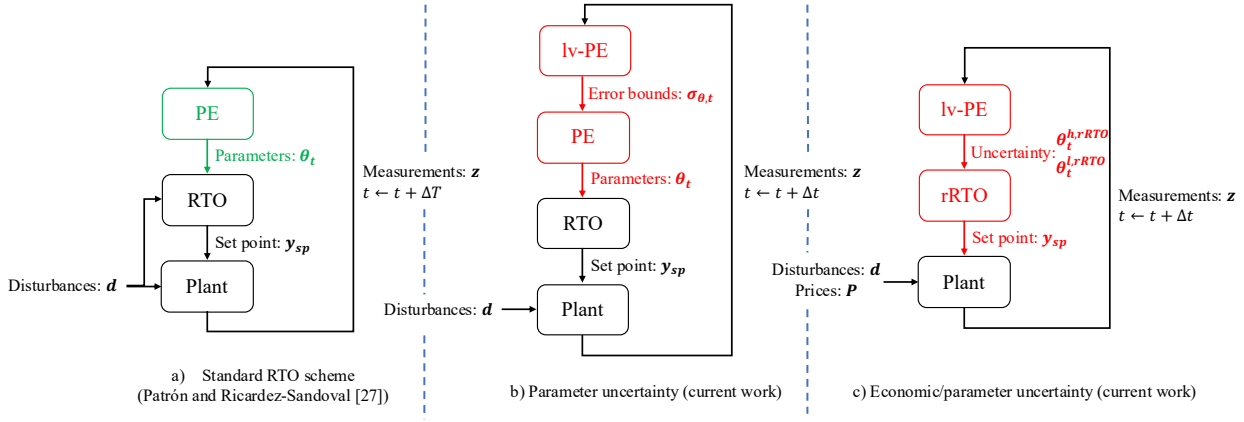

Figure 1: Potential RTO architectures. a) parameter uncertainty considered; previous PCC works omitted green block and no uncertainty, b) parameter uncertainty considered using the method in section 2.1, c) parameter and price uncertainties considered using the method in section 2.2. Novel layers considered in this study are shown in red.

RTO-operated systems work in the manner depicted in Figure 1a. The RTO computes controlled variable set points, which are passed to the controller. The controller (which could be PID, MPC, NMPC, etc., omitted for brevity) acts by receiving feedback from the plant in the form of state measurements and regulating the plant towards the RTO-defined set point through the manipulated variables, making the scheme closed loop. On a longer timescale, known as the RTO period ΔT, the parameter estimation (PE) problem is executed such that uncertain parameters are updated and the RTO can re-compute the set points under changes in operating conditions.

Generally, RTO is used to optimize process economics such that the process operating conditions can be adjusted as a response to varying disturbances. The formulation for RTO economic optimization at time t is expressed as follows:

$$\begin{aligned} &\min_{\hat{\boldsymbol{y}}_t} \Phi\,(\hat{\boldsymbol{x}}_t) \\ &s.t. \\ &\boldsymbol{f_s}(\hat{\boldsymbol{x}}_t, \hat{\boldsymbol{y}}_t, \boldsymbol{u_t}, \boldsymbol{d_t}, \boldsymbol{\theta_t}) = \boldsymbol{0} \\ &\boldsymbol{g_s}(\hat{\boldsymbol{x}}_t, \boldsymbol{u_t}, \boldsymbol{d_t}) \leq \boldsymbol{0} \\ &\boldsymbol{y^l} \leq \hat{\boldsymbol{y}}_t \leq \boldsymbol{y^h} \\ &\boldsymbol{u^l} \leq \boldsymbol{u_t} \leq \boldsymbol{u^h} \end{aligned} \tag{1}$$

where $\Phi \in \mathbb{R}$ is the economic objective function to be optimized (minimization of process cost is taken as convention in this study). $\hat{\boldsymbol{x}}_t \in \mathbb{R}^{n_x}$, $\hat{\boldsymbol{y}}_t \in \mathbb{R}^{n_y}$, $\boldsymbol{u_t} \in \mathbb{R}^{n_u}$, $\boldsymbol{d_t} \in \mathbb{R}^{n_d}$ and $\boldsymbol{\theta_t} \in \mathbb{R}^{n_\theta}$ are the state predictions, controlled variable predictions (i.e., set points), manipulated variables, measurable disturbance variables, and uncertain parameters, respectively, at the solution time t. $\boldsymbol{y^l}$ and $\boldsymbol{y^h} \in \mathbb{R}^{n_y}$ are the lower and upper bounds for the controlled variables, respectively; similarly, $\boldsymbol{u^l}$ and $\boldsymbol{u^h} \in \mathbb{R}^{n_u}$ are the lower and upper bounds for the manipulated variables, respectively. $\boldsymbol{f_s}$: $\mathbb{R}^{n_u} \times \mathbb{R}^{n_d} \times \mathbb{R}^{n_\theta} \longrightarrow \mathbb{R}^{n_x} \times \mathbb{R}^{n_y}$ is a steady-state process model, which maps the inputs, disturbances, and parameters to the state and controlled variables. $\boldsymbol{g_s}$: $\mathbb{R}^{n_x} \times \mathbb{R}^{n_u} \times \mathbb{R}^{n_d} \longrightarrow \mathbb{R}^{n_g}$ are any additional inequality constraints imposed on the RTO problem that must be satisfied. The outputs (i.e., decision variables) from the RTO problem are $\hat{\boldsymbol{y}}_t$, such that the controlled variable predictions can be passed to the control layer as set points in the manner depicted in Figure 1a. The inputs for the RTO problem are the disturbances ($\boldsymbol{d_t}$) and the model parameters ($\boldsymbol{\theta_t}$) at time t; thus, these must be known prior to solving problem (1).

In the context of energy systems, Φ could represent emissions, energy consumption, or a comprehensive economic function. Moreover, measurable disturbances ($\boldsymbol{d_t}$) may include changes in electricity demands, fuel grades, or regulatory constraints. The uncertain parameters ($\boldsymbol{\theta_t}$) can include any experimentally determined phenomenological constants (e.g., kinetics, thermodynamics, and equilibrium) or unmeasured disturbances (e.g., compositions) that are built into the model $\boldsymbol{f_s}$. While the uncertain parameters are inherent to the process model, the unmeasured disturbances

are external (i.e., a function of factors outside the plant). For PCC, model parameters can include activity coefficients or reaction kinetic parameters, while unmeasured disturbances can include inlet compositions. In process systems, the uncertain model parameters and unmeasured disturbances can both be treated as uncertain parameters, thus necessitating an estimation scheme.

2.1. Low-variance parameter estimation (lv-PE)

As mentioned above, uncertain parameters are treated as inputs to the RTO model. Rather than assuming these parameters are fixed, they are updated at regular intervals in the two-step RTO implementation. Moreover, there are many external factors that can be considered as unmeasured disturbances in energy and CO_2 capture systems, which are highly dependent on human behaviour, environmental factors, and process inputs. For instance, energy demands may vary diurnally (Patrón and Ricardez-Sandoval, 2022a), government production incentives may change (Patrón and Ricardez-Sandoval, 2020a), or process inputs material grades and types may fluctuate (Hodžić et al., 2020; Loeffler, 2014). These unpredictable changes may result in changes in flue gas composition, which may be difficult or inaccurate to measure. These unmeasured disturbances can also be treated as uncertain parameters. The uncertain parameters $\boldsymbol{\theta_t}$ as defined in this work, are time-invariant, i.e., they do not change as an explicit function of the sampling interval but can vary because of the external factors, e.g., changes in the operating conditions. As such, they are updated every RTO period ΔT prior to the set point update. Moreover, the uncertain parameters are bounded such that they are assumed to materialize within a certain range determined *a priori* and constraints on their estimates can be considered in the PE problem to provide a search space.

Problem (1) requires solving a PE problem that provides estimates for $\boldsymbol{\theta_t}$ so the RTO problem can be solved at time t. In the estimation problem $\boldsymbol{z_t} \in \mathbb{R}^{n_z}$ denotes the process measurements; these are sampled from the plant every interval Δt. Measurement samples are required before the parameters can be updated such that statistical properties of the measurements can be computed. The sample statistics are used to reconcile the plant and the model by formulating a least-squares optimization problem that minimizes the differences between the plant measurements and the model measurement predictions. The PE formulation at time t is as follows:

$$
\begin{aligned}
&\min_{\boldsymbol{\theta_t}} \|\hat{\boldsymbol{z}}_{\boldsymbol{t}} - \bar{\boldsymbol{z}}_{\boldsymbol{t}}\|_{\boldsymbol{K_t}^{-1}}{}^2 \\
&s.t. \\
&\boldsymbol{f_s}\left(\hat{\boldsymbol{x}}_{\boldsymbol{t}}, \hat{\boldsymbol{y}}_{\boldsymbol{t}}, \bar{\boldsymbol{u}}_{\boldsymbol{t}}, \bar{\boldsymbol{d}}_{\boldsymbol{t}}, \boldsymbol{\theta_t}\right) = \mathbf{0} \\
&\boldsymbol{h_s}\left(\hat{\boldsymbol{x}}_{\boldsymbol{t}}, \bar{\boldsymbol{u}}_{\boldsymbol{t}}, \bar{\boldsymbol{d}}_{\boldsymbol{t}}\right) = \hat{\boldsymbol{z}}_{\boldsymbol{t}} \\
&\boldsymbol{g_s}\left(\hat{\boldsymbol{x}}_{\boldsymbol{t}}, \bar{\boldsymbol{u}}_{\boldsymbol{t}}, \bar{\boldsymbol{d}}_{\boldsymbol{t}}\right) \leq \mathbf{0}
\end{aligned}
\tag{2}
$$

$$\boldsymbol{\theta}^{l,pe} \leq \boldsymbol{\theta}_t \leq \boldsymbol{\theta}^{h,pe}$$

where $\boldsymbol{f_s}$, $\boldsymbol{g_s}$, and all variables are defined as in problem (1). $\boldsymbol{h_s}$: $\mathbb{R}^{n_x} \times \mathbb{R}^{n_u} \times \mathbb{R}^{n_d} \longrightarrow \mathbb{R}^{n_z}$ denotes an observer function between the model state, inputs, measurable disturbances, and predicted measurements. $\bar{\boldsymbol{z}}_t$ and $\hat{\boldsymbol{z}}_t \in \mathbb{R}^{n_z}$ are the sample-averaged and the model-predicted process measurements, respectively. The PE problem requires a sample of measurements of size M, denoted as $\{\boldsymbol{z_{t-i}}\}_{i=0}^{M}$, which is used to calculated averaged quantities $\bar{\boldsymbol{z}}_t = \frac{1}{M}\sum_{i=0}^{M} \boldsymbol{z_{t-i}}$. $\boldsymbol{K_t} \in \mathbb{R}^{n_z \times n_z}$ is the measurement covariance matrix, which can be computed from the measurement sample; the inverse of this matrix is used to weight the objective function, which minimizes the quadratic form of the difference of sample averages and model predictions. The inverse covariance matrix weighs the objective function such that measurements with high variance are given less weight and measurements with low variance are given more weight; it also scales terms such that measurements with different magnitudes can be used within the same objective function. The quadratic form and inverse covariance weighting are used as the objective in formulation (2) and denoted as $\| \|_{\boldsymbol{K_t}^{-1}}^2$. Further, $\left(\bar{\boldsymbol{u}}_t = \frac{1}{M}\sum_{i=0}^{M} \boldsymbol{u_{t-i}}\right) \in \mathbb{R}^{n_u}$ and $\left(\bar{\boldsymbol{d}}_t = \frac{1}{M}\sum_{i=0}^{M} \boldsymbol{d_{t-i}}\right) \in \mathbb{R}^{n_d}$ are the time-averaged process inputs and measurable disturbances, respectively, which are provided to the PE problem. $\boldsymbol{u_t}$ and $\boldsymbol{d_t}$ are readily available as the control actions and measured disturbances prior to the PE problem are defined by the control scheme and measured, respectively; thus, they are the inputs to the PE problem (2). Moreover, $\hat{\boldsymbol{x}}_t$ and $\hat{\boldsymbol{y}}_t$ are the state and controlled variables predictions, respectively, produced by the steady-state model $\boldsymbol{f_s}$. $\boldsymbol{\theta_t}$ are the uncertain parameters, which are to be estimated (i.e., the decision variables to formulation (2)). $\boldsymbol{\theta}^{l,pe}$ and $\boldsymbol{\theta}^{h,pe}$ are the lower and upper bounds for the uncertain parameters, respectively, which are user-defined. The uncertain parameters can be classified into two subsets $\boldsymbol{\theta} = [\boldsymbol{\theta_d} \quad \boldsymbol{\theta_p}]^T$. $\boldsymbol{\theta_d} \in \mathbb{R}^{n_{\theta_d}}$ are the uncertain parameters that come from external sources (e.g., unmeasured disturbance) while $\boldsymbol{\theta_p} \in \mathbb{R}^{n_{\theta_p}}$ are parameters that are inherent to the process model (e.g., physical properties); accordingly, $n_\theta = n_{\theta_d} + n_{\theta_p}$.

As mentioned previously, the estimated uncertain parameters ($\boldsymbol{\theta_t}$) are passed to the RTO formulation in equation (1) at time t as depicted in Figure 1a and can also be passed to a controller with a matching model to the RTO. These are updated at every RTO period ΔT such that the plant and model are consistently being reconciled. However, the estimation scheme requires noisy measurements ($\boldsymbol{z_t}$) that will inherently include noise that may be propagated from the measurements to the parameter estimates. If the RTO economics are sensitive to these estimated quantities,

substantial economic losses may occur. In a system such as PCC, this could manifest through increased energy consumption, resource use, or emissions, which are costly and have prices that accrue over time. Accordingly, the low variance estimation (lv-PE) method proposed in Patrón and Ricardez-Sandoval (2022b) is deployed herein to abate the propagation of noise from measurements to estimates.

Algorithm 1: lv-PE	
	Every RTO period ΔT: initialize $j = 1$.
1.	Acquire $M + 1$ measurement samples, compute M parameter estimate samples $\{\widehat{\boldsymbol{\theta}}_0\}_{i=1}^{M}$ using all measurements and formulation (2).
2.	Remove measurement type z_j and compute M parameter estimate samples $\{\widehat{\boldsymbol{\theta}}\}_{i=1}^{M}$.
a.	If estimate standard deviation $\boldsymbol{\sigma_{\theta,j}} < \boldsymbol{\sigma_{\theta,j+1}}$: remove z_j from measurement set.
b.	Else: retain z_j in measurement set.
3.	$j \pm 1$
a.	If $j = n_z$ or observability is lost: go to step 4.
b.	Else: return to step 2.
4.	Execute final PE problem with best measurement set, apply to plant.
5.	Filter plant estimates through tightest $\boldsymbol{\sigma_{\theta,j}}$.

To summarize, the lv-PE algorithm 1 is used to determine a measurement set that results in low errors in $\boldsymbol{\theta_t}$ *a priori* to the PE problem. Within the lv-PE algorithm, many PE problems are executed offline via a bootstrapping method that generates parameter estimate samples that correspond to different measurement sets; this is done by excluding individual measurements sequentially from formulation (2) as explained in step 2 of algorithm 1. The standard deviations in estimates for each measurement set are compared to determine which measurements result in the highest precision; this measurement set is chosen for the actual (i.e., applied to the plant) PE problem. Additionally, lv-PE uses the statistics acquired by the bootstrap to provide error bounds and filter the estimates $\boldsymbol{\theta_t}$ *a posteriori* to the online PE problem as shown in step 5 of algorithm 1. Interestingly, lv-PE has yet to be applied to a large-scale system like PCC; thus, its benefit on this class of systems with many inputs and slow dynamics is unknown. PCC, for which uncertainty has not been addressed in online economic optimization, is well-suited to lv-PE as it has infrequent set point changes resulting in long periods at steady state. The measurements acquired at steady state will enable the repeated data collection required for the bootstrapping that lv-PE entails; as such, high-fidelity parameter estimates can be computed to operate the system near its true optima. Moreover, the mechanistic PCC has been shown to exhibit parameter sensitivity (Cerrillo-Briones and Ricardez-Sandoval, 2019; Hughes et al., 2022; Patron and Ricardez-

Sandoval, 2020b). The exchange of information between the lv-PE and PE layers are shown in Figure 1b while the full algorithm is omitted for brevity and can be found elsewhere (Patrón and Riacrdez-Sandoval, 2022b).

2.2. Robust RTO (rRTO) formulation

In addition to the uncertain parameters ($\boldsymbol{\theta_t}$), the RTO presented in equation (1) can also manifest uncertainty in the economics. In this case, the economic function is denoted as $\Phi(\hat{\boldsymbol{x}}_t, \boldsymbol{P_t})$ where $\boldsymbol{P_t} \in \mathbb{R}^p$ are the economic uncertainties at time t. When economic uncertainty occurs, the operator may want to find an operating point that accommodates a range of uncertain economic scenarios. For instance, when the economics ($\boldsymbol{P_t}$) and parameters ($\boldsymbol{\theta_t}$) are frequently fluctuating, a single solution that works well regardless of the actual realization of uncertainties that happen in the future may be advantageous (i.e., a robust solution that is also suitable for the short-term future); however, this robust solution may sacrifice performance if uncertainties remain fixed and an accurate parameter estimation scheme is available. As mentioned above, previous studies have considered economic robustness in PCC (Wu et al., 2015; Xuan et al., 2022; Zantye et al., 2019); however, those schemes make decisions in scheduling and planning timescales, not in real-time. In this economically robust paradigm, one can also address uncertainty in the parameters by bypassing the PE problem (2) and formulating a problem that is robust to both parameter and economic uncertainties.

To achieve RTO robustness with uncertainty in both economics and model parameters (in contrast to uncertainty in parameters only as in section 2.2.), the multi-scenario approach can be employed where various model realizations are solved. This approach has been employed in PCC design (Cerrillo-Briones and Ricardez-Sandoval, 2019) and control (Patron and Ricardez-Sandoval, 2020b), but never considered in an online real-time economic optimization context such as RTO. As such, the multi-scenario approach is applied for robust RTO (rRTO) herein at time t as follows:

$$
\begin{aligned}
&\min_{\hat{\boldsymbol{y}}_t} \textstyle\sum_{j=1}^{n_r} \omega_{t,j} \Phi\left(\hat{\boldsymbol{x}}_{t,j}, \boldsymbol{P}_{t,j}\right) \\
&s.t. \\
&\boldsymbol{f}_{s,j}\left(\hat{\boldsymbol{x}}_{t,j}, \hat{\boldsymbol{y}}_{t,j}, \boldsymbol{u}_{t,j}, \boldsymbol{d}_t, \boldsymbol{\theta}_{t,j}\right) = \boldsymbol{0} && \forall j \in \{1, \dots, n_r\} \\
&\boldsymbol{g}_{s,j}\left(\hat{\boldsymbol{x}}_{t,j}, \boldsymbol{u}_{t,j}, \boldsymbol{d}_t\right) \leq \boldsymbol{0} && \forall j \in \{1, \dots, n_r\} \quad (3) \\
&\boldsymbol{y}^{\boldsymbol{l}} \leq \hat{\boldsymbol{y}}_{t,j} \leq \boldsymbol{y}^{\boldsymbol{h}} && \forall j \in \{1, \dots, n_r\} \\
&\boldsymbol{u}^{\boldsymbol{l}} \leq \boldsymbol{u}_{t,j} \leq \boldsymbol{u}^{\boldsymbol{h}} && \forall j \in \{1, \dots, n_r\} \\
&\hat{\boldsymbol{y}}_{t,1} = \cdots = \hat{\boldsymbol{y}}_{t,j} = \cdots = \hat{\boldsymbol{y}}_{t,n_r}
\end{aligned}
$$

where all variables and functions are the same as in formulation (1) with the additional index $j \in \{1, \dots, n_r\}$. This index represents individual scenarios being considered, which generates various instances of the process model; each instance j represents a realization of the uncertain parameters. Accordingly, the last constraint in formulation (3)

ensures the set point decision variables for all realizations are equivalent. Through the set point equivalence, a single set point is found that is optimal for all realizations; this is the set point that is provided to the control layer as shown in Figure 1c.

To choose which uncertainty combinations are featured in j, the uncertain parameters are assumed to manifest within $[\boldsymbol{\theta}_t^{l,rRTO}, \boldsymbol{\theta}_t^{h,rRTO}]$, which represents the lower and upper bounds of the parameter uncertainty region, respectively. As with the uncertain parameters, the objective function Φ has the dependence on $\boldsymbol{P}_{t,j}$, which can manifest within the region $[\boldsymbol{P}_t^{l}, \boldsymbol{P}_t^{h}]$. Accordingly, n_r, which corresponds to the index j, is the number of scenarios considered within these regions upon discretization of the intervals. Note that the bounds of the regions are indexed in t such that they may expand or contract across RTO periods to accommodate for changing levels of uncertainty. The scenarios encompass the bounds of the uncertainty region; however, the choice of discretization for the uncertainty regions is a user-defined choice that balances computational efficiency with robustness. As more scenarios are included, the model size grows but represents a better approximation of the continuous uncertainty region between the bounds.

Owing to the parameter and economic uncertainty region discretization described above, the economics of the various model realizations are minimized jointly in the rRTO objective function in equation (3). Each objective function term is weighed by $\omega_{t,j}$, which corresponds to the probability of a given realization occurring such that $\sum_{j=1}^{n_r} \omega_{t,j} = 1$; these must be established *a priori* based on the underlying statistical distribution that the uncertain parameters and economics obey. As with the uncertainty regions above, the weights are indexed in t to reflect changing realization probabilities.

While $\boldsymbol{P}_t^{l}$ and $\boldsymbol{P}_t^{h}$ must be established based on knowledge of the economic process incentives, the size of the parameter uncertainty region (defined by $\boldsymbol{\theta}_t^{l,rRTO}$, $\boldsymbol{\theta}_t^{h,rRTO}$) is typically difficult to quantify and is based on process knowledge rather than a systematic uncertainty quantification method. However, the lv-PE method presented Patrón and Ricardez-Sandoval (2022b) presents a bootstrap method that acquires data at every sampling period Δt to quantify the parameter uncertainty region via the parameter standard deviations generated therein. This data-driven approach provides uncertainties that accurately reflect potential parameter realizations while avoiding undue conservatism, which would hinder performance (e.g., Patrón and Ricardez-Sandoval, 2020b). Without such an uncertainty quantification method, the solution may be overly or insufficiently robust. As such, the parameter uncertainty region for the rRTO problem is defined as $\left[\boldsymbol{\theta}_t^{l,rRTO}, \boldsymbol{\theta}_t^{h,rRTO}\right] = [\overline{\boldsymbol{\theta}}_t - \frac{\tau}{\sqrt{M}}\boldsymbol{\sigma}_{\boldsymbol{\theta}_t}, \overline{\boldsymbol{\theta}}_t + \frac{\tau}{\sqrt{M}}\boldsymbol{\sigma}_{\boldsymbol{\theta}_t}]$ where $\overline{\boldsymbol{\theta}}_t$, $\boldsymbol{\sigma}_{\boldsymbol{\theta}_t}$, and M are the

sample mean, standard deviation and size, respectively, as defined by the algorithm in our previous work (Patrón and Ricardez-Sandoval, 2022b). As the quantities acquired in the lv-PE procedure are indexed in time t to accommodate for changing levels of uncertainty across RTO periods, these bounds also reflect changing uncertainty. Moreover, τ allows for the use of confidence intervals to reflect the error tolerance of the user and can be retrieved from a two-sided t-distribution; this gives statistical significance to the robustness in formulation (3). The parameter uncertainty region $\left[\boldsymbol{\theta}_t^{l,rRTO}, \boldsymbol{\theta}_t^{h,rRTO}\right]$ differs from the PE optimization bounds in section 2.1 as it is acquired from the lv-PE algorithm while PE bounds are defined based on process knowledge. The rRTO algorithm 2 is summarized below. In summary, parameter uncertainty bounds are acquired using the statistics from the bootstrapping method in lv-PE; these quantify the model uncertainty region in step 2 of algorithm 2. Using this uncertainty, a multi-scenario optimization problem (3) is solved in step 3 such that the RTO is optimal on aggregate across potential parameter realizations and robust set points can be conveyed to the PCC plant.

Algorithm 2: rRTO	
	Every RTO period ΔT. Choose n_r and τ.
1.	Execute lv-PE algorithm 1 and acquire $\overline{\boldsymbol{\theta}}_t$ and $\boldsymbol{\sigma}_{\boldsymbol{\theta}_t}$ for most precise measurement set.
2.	Construct uncertainty region as $\left[\boldsymbol{\theta}_t^{l,rRTO}, \boldsymbol{\theta}_t^{h,rRTO}\right] = [\overline{\boldsymbol{\theta}}_t - \frac{\tau}{\sqrt{M}}\boldsymbol{\sigma}_{\boldsymbol{\theta}_t}, \overline{\boldsymbol{\theta}}_t + \frac{\tau}{\sqrt{M}}\boldsymbol{\sigma}_{\boldsymbol{\theta}_t}]$.
3.	Discretize uncertainty region according to n_r and embed into problem (3)
4.	Solve rRTO problem and apply to plant.

By bypassing the PE step in problem (2) and only conveying parameter bounds to problem (3), the rRTO formulation finds robust solutions that account for economics fluctuations and parameters uncertainties. Accordingly, the rRTO formulation (3) can be deployed instead of the hierarchical approach that uses formulations (1) and (2). This exchange of information is shown in Figure 1c.

3. Scheme implementation and assessment

A pertinent application of the methods outlined in previous sections is PCC; a technology whose global industrial adoption is currently limited by its unfavourable process economics. As depicted in Figure 2, the PCC plant consists of two main units: an absorber and a stripper. The absorber receives flue gas and a lean (i.e., without CO_2) amine solution in a counter-current arrangement such that they contact and incite a reactive absorption mechanism. The gas without CO_2 is vented from the absorber while the rich (i.e., with CO_2) solvent passes to the stripper via a heat exchanger. The stripper requires a reboiler to further heat the rich solution and separate the CO_2 from the amine along

the stripper column. The CO_2 is further purified through a condenser as shown in Figure 2, whereby any evaporated solution is removed and recycled to the stripper. In the bottom of the column, purified amine solvent is recycled to the absorber section via a buffer tank where makeup solvent and water may be added.

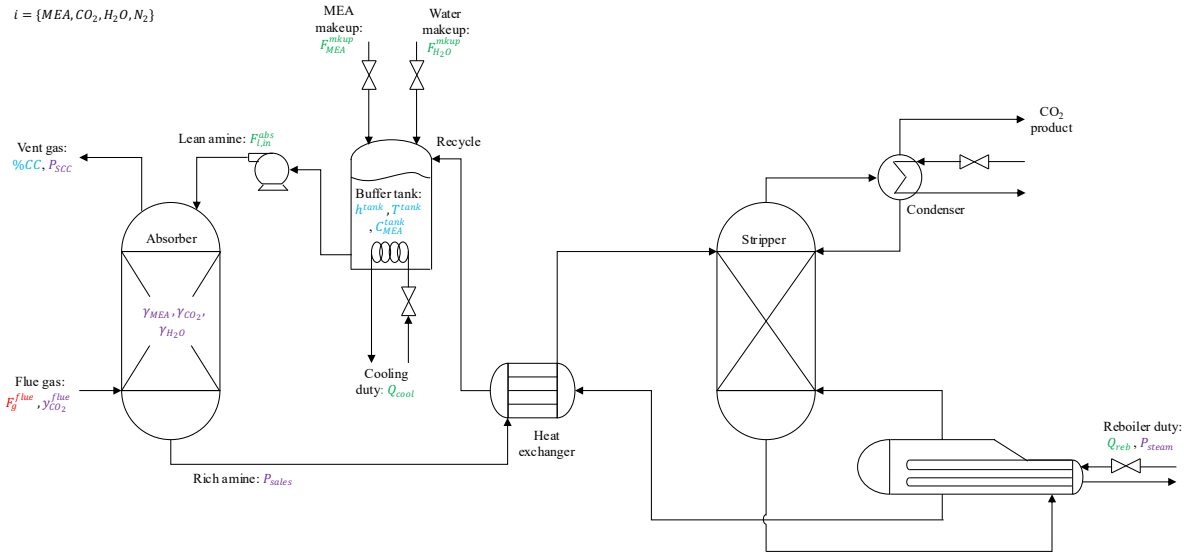

Figure 2: PCC plant. Blue font denotes controlled variables, purple font denotes the uncertainties, green font denotes manipulated variables, and red font denotes disturbance variables.

RTO and the estimation schemes require a model to formulate their respective optimization problems. Herein, a mechanistic model for a PCC absorber section, denoted $\boldsymbol{f_s}$, is used to test the present estimation approaches is used; this model is outlined in the supplementary information and was validated in Patrón and Ricardez-Sandoval (2022a). The PCC model requires manipulated variables as inputs. These are defined as the vector $\boldsymbol{u} = \left[F_{l,in}^{abs} \quad F_{MEA}^{mkup} \quad F_{H_2O}^{mkup} \quad Q_{cool} \quad Q_{reb}\right]^T$, whereby the flowrate from tank to absorber is regulated through a variable-speed pump, the makeup flowrates are regulated using valves, the cooling duty is regulated through cooling water flowrate to a coil in the tank, and the reboiler duty is regulated through steam pressure to the reboiler coils. The manipulated variables are used to regulate the controlled variables, which are denoted as $\boldsymbol{y} = [\%CC \quad C_{MEA}^{tank} \quad h^{tank} \quad T^{tank}]^T$. The controlled variables include the carbon captured rate, the MEA concentration in the tank, the tank liquid level, and the tank temperature. The nominal values for the manipulated variables and controlled variables are $\boldsymbol{u_{nom}} = [32.17\, mol/s \quad 0.0002\, mol/s \quad 0.2\, mol/s \quad -139{,}000\, W \quad 153{,}500\, W]^T$ and $\boldsymbol{y_{nom}} = [96.23\% \quad 4847\, mol/L \quad 1\, m \quad 314\, K]^T$, respectively.

As noted earlier, uncertain parameters can be segmented into physical properties and unmeasured disturbances, which will be assessed individually through their respective estimates on the RTO scheme. In the PCC plant, both the flue

gas flowrate and CO_2 content entering the absorber are typical disturbances. Both disturbances are typically measurable in power plants (e.g., via a flowmeter and a katharometer, respectively). Although the accuracy of the katharometer is generally adequate for monitoring of emissions (e.g., $\pm 0.5\ mol\%$ in absolute terms; ABB, 2003), it may not be adequate for RTO where the optimum is sensitive to the carbon content of the flue gas. Accordingly, an estimation scheme is proposed for the flue gas CO_2 and H_2O concentrations (i.e., $\boldsymbol{\theta_d} = \left[y_{CO_2}^{flue} \quad y_{H_2O}^{flue}\right]^T$) while flue gas flowrate is assumed to be a measured disturbance (i.e., $\boldsymbol{d} = \left[F_0^g\right]^T$). The estimated unmeasured disturbances are treated as uncertain parameters ($\boldsymbol{\theta_d}$) and provided to the RTO layers such that high-fidelity composition estimates are generated and lead to high-fidelity set points. Only these two component fractions are taken as disturbances as the nitrogen fraction is fixed since it is inert in the upstream combustion process, and the MEA is assumed to be unevaporable. The nominal values for the measurable and unmeasured disturbances are $\boldsymbol{d_{nom}} = [4.012\ mol/s]^T$ and $\boldsymbol{\theta_{d,nom}} = [0.175\ mol/mol \quad 0.025\ mol/mol]^T$, respectively. Moreover, activity coefficients are assumed to be the cause of the parametric uncertainties in the PCC model and, as such, are considered uncertain parameters (i.e., $\boldsymbol{\theta_p} = [\gamma_{MEA} \quad \gamma_{CO_2} \quad \gamma_{H_2O}]^T$). While these parameters are assumed to be constant in the process model (i.e., time-invariant), their true values are not precisely known and are designed to capture non-idealities in fluid behaviour, which may vary over time as the operation of PCC is highly nonlinear. Accordingly, it is important to update the parameters on a regular basis as operating conditions change. The effect of uncertainty via the activity coefficients has been previously explored in the context of PCC design (Cerrillo-Briones and Ricardez-Sandoval, 2019) and control (Patron and Ricardez-Sandoval, 2020b); however, it has not been addressed in RTO. The nominal values for the uncertain parameters are $\boldsymbol{\theta_{p,nom}} = [0.381 \quad 0.677 \quad 0.974]^T$).

This PCC model was implemented in the Pyomo (Hart et al., 2011) modelling environment for Python. The absorber column was discretized with ten backward finite difference elements in the axial domain (i.e., $n_{fez} = 10$); this discretization was chosen such that the models yielded high-accuracy predictions while remaining relatively quick to solve. The discretization scheme results in a model size of 116 states and 1,977 algebraic variables. The model is solved using the interior-point method IPOPT (Wächter and Biegler, 2005) on an Intel core i7-4770 CPU @ 3.4 GHz processing unit.

The model presented herein was validated across a wide range of operating conditions in our previous study (Patrón and Ricardez-Sandoval, 2022a) and found to have an error across all model outputs of $< 4\%$ with respect to

experimental data and an error of $< 8\%$ with respect to the implementation of the same model by Harun et al. (2012). The reader is asked to refer to this work for further details on model validation.

3.1. RTO economics and constraints

The RTO objective function in formulation (1) for the PCC system used in this study was first introduced in Patrón and Ricardez-Sandoval (2022a) and uses the steady state model $\boldsymbol{f_s}$ also introduced therein, which is presented in the supplementary material for brevity. The economic objective is defined as follows:

$$\phi = P_{MEA}\dot{m}_{MEA}^{mkup} + P_{sales}(\dot{m}_{CO_2,in}^{g} - \dot{m}_{CO_2,out}^{g}) + P_{CO_2}\dot{m}_{CO_2,out}^{g} + P_{steam}Q_{reb} \quad (4)$$

where P_{MEA}, P_{sales}, P_{CO_2} and P_{steam} are the MEA makeup (i.e., fresh MEA added to the system) price, the CO_2 sales price, the social cost of carbon (SCC), and the price of steam, respectively, which are the most important economic aspect of PCC. These are multiplied by their corresponding mass flowrates ($\dot{m}$) or duties (Q). These prices are outlined in Table 1 as proposed in our previous work (Patrón and Ricardez-Sandoval, 2022a):

Table 1: Prices used in RTO and energy penalty assessment.

Term	Value	Source
MEA (P_{MEA})	2420 $\$CAD/tn\ fresh\ MEA$	Straathof and Bampouli (2017)
Sales (P_{sales})	-50 $\$CAD/tn\ CO_2\ sold$	Nwaoha and Tontiwachwuthikul (2019)
CO_2 (P_{CO_2})	176 $\$CAD/tn\ CO_2\ removed$	Nordhaus (2017)
Steam (P_{steam})	0.065 $\$CAD/kWh$	Karimi et al. (2011)
Electricity (P_{elec})	0.115 $\$CAD/kWh$	OEB (2021)

As established in previous works (e.g., Danaci et al., 2021), the steam requirements of the PCC system comprise much of the operating cost while the solvent requirements are also significant. The steam pressure in a pilot-scale PCC reboiler is typically 135−150 kPa (Artanto et al., 2011) and the price of steam to PCC is denominated in terms of kWh as it represents the main energy term to the process. In contrast, condenser cooling water and makeup process water costs are orders of magnitude smaller, thus they are not considered in the economic function (4). Moreover, the SCC is used to consider the negative externalities (e.g., effects on health and environmental outcomes) of carbon emission, thus further incentivizing capture by using a more stringent cost over a cheaper carbon tax. Additionally, CO_2 sales consider a potential carbon economy in which captured product can be sold for profit. To further constrain formulation (1), the following bounds are imposed on the controlled variables:

$$
\begin{aligned}
&0 \le \%CC \le 100 \\
&3000 \le C_{MEA}^{tank}\ (mol/L) \le 6000 \\
&0.05 \le h^{tank}(m) \le 1.95 \\
&300 \le T^{tank}\ (K) \le 345
\end{aligned}
\tag{5}
$$

where the $\%CC$ constraint ensures the model prediction stays within a physically realistic range, the C_{MEA}^{tank} indirectly constrains the reboiler heat duty and MEA makeup that affect the MEA concentration in the buffer tank, the T^{tank} ensures the absorber feed temperature is within typical operating limits, and the h^{tank} constraint ensures the buffer tank does not empty or overflow.

Likewise, the following bounds are imposed on the manipulated variables to ensure that the control variables corresponding to the steady-state set points are within the physical limits of the instrumentation:

$$
\begin{aligned}
&0 \le F_{l,in}^{abs}\ (mol/s) \le 100 \\
&0 \le F_{MEA}^{mkup}\ (mol/s) \le 1 \\
&0 \le F_{water}^{mkup}\ (mol/s) \le 1 \\
&-500{,}000 \le Q_{cool}\ (W) \le 0
\end{aligned}
\tag{6}
$$

Equations (5) and (6) constrain the RTO feasible search space and keep the PCC operation within realistic operational limits. Moreover, the foremost factor motivating the deployment of RTO is the process economics; thus, each scheme and scenario will be analyzed by their cumulative cost $C(\$CAD)$ across N RTO periods tested, defined as follows:

$$
C_{PCC} = \Delta T \sum_{i=0}^{N} \phi_i \tag{7}
$$

where $\phi_i(\$CAD/hour)$ is the price of operating the PCC according to equation (4) at every RTO period i.

In addition to considering the cost of the PCC system, the effect that the reboiler has on the upstream power plant must also be accounted for. The reboiler requires steam that comes from the power plant, resulting in a reduction of the power generation capacity and high cost (Zhang et al., 2017). This is accounted for by considering the cumulative energy penalty $C_{energy}(\$CAD)$ across N RTO periods tested in each scenario, defined as follows:

$$
C_{energy} = \Delta T \sum_{i=0}^{N} Q_{reb,i}(P_{elec} - P_{steam})\eta \tag{8}
$$

where $Q_{reb,i}(kW)$ denotes the reboiler duty, P_{elec} and $P_{steam}(\$CAD/kWh)$ denote the electricity price rate and the steam price rate, respectively, while $\eta = 0.4$ (Mac Dowell and Shah, 2013) denotes the efficiency of converting steam to electricity in the power plant. The difference between energy sales and steam prices corresponds to the energy price

markup upon sale. These are multiplied by the reboiler duty through an efficiency factor to quantify the profit loss incurred by using the steam in the PCC reboiler instead of using it in the power plant turbines.

In addition to quantifying the potential economic and energy effects of the RTO. The environmental effects are also of utmost importance. To do this, the cumulative mass of CO_2 emitted $m_{CO_2}^{emitted}(tn)$ over N RTO operating periods is calculated as follows:

$$m_{CO_2}^{emitted} = \Delta T M_{CO_2} \sum_{i=0}^{N} F_{g,i}^{vent} y_{CO_2,i}^{vent} \tag{9}$$

where $F_{g,i}^{vent}(mol/hr)$ and $y_{CO_2,i}^{vent}(mol/mol)$ are the vent gas flowrate and CO_2 fraction for each RTO period, respectively, and $M_{CO_2}(tn/mol)$ is the molar mass of CO_2. In addition, an influencing factor in the PCC economics is the amount of MEA makeup added in the tank (Patrón and Ricardez-Sandoval, 2022a). Accordingly, this is also considered in the assessment of the RTO across N RTO periods tested in each scenario, i.e.,

$$m_{MEA}^{mkup} = \Delta T M_{MEA} \sum_{i=0}^{N} F_{MEA,i}^{mkup} \tag{10}$$

where $m_{MEA}^{mkup}(tn)$ is the amount of makeup MEA used and $M_{MEA}(tn/mol)$ is the molar mass of MEA.

3.2. PE measurements and constraints

The present analysis assumes that only 12 measurements are available for estimation, which are denoted as $\boldsymbol{z} = \left[\boldsymbol{C_H^g}^T \quad \boldsymbol{C_0^l}^T \quad T_{g,0} \quad T_{g,H} \quad T_{l,0} \quad T_{l,H}\right]^T$. These include the liquid ($\boldsymbol{C_0^l}$) and gas ($\boldsymbol{C_H^g}$) compositions and temperatures at the bottom and top of the absorber column. Only a single set of gas and liquid absorber concentration measurements along the absorber height are used; thus, it is assumed that these are accessible at the column top and bottom outlets, respectively. This is done as sampling of inlet and outlet streams is more practical than sampling along the column height; moreover, good estimate quality was observed with these sampling locations (Patrón and Ricardez-Sandoval, 2022a). The sample size is assumed to be $M = 40$ such that the estimation schemes can provide good estimates while not incurring any delays in the execution of the RTO. This sample size was chosen based on preliminary simulations and ensures significant measurement averaging occurs such that increasing beyond this size makes little difference. Conversely, significantly smaller sample sizes may allow noise propagation as they do not benefit from averaging effects. In addition to these measurements, the following bounds are also given to the PE problem (2) in the case of uncertain model parameters ($\boldsymbol{\theta_p}$):

$$0 < \gamma_{MEA}, \gamma_{CO_2}, \gamma_{H_2O} < 2 \tag{11}$$

The upper bound of equation (11) is chosen as to match the activity coefficient range for mixed amine solutions loaded with CO_2 presented in Kaewsichan et al. (2001). Furthermore, the following constraints are included in the DE problem (2) in the case of unmeasured disturbances ($\boldsymbol{\theta_d}$):

$$\begin{aligned} &y_{CO_2}^{flue} + y_{H_2O}^{flue} = 0.2 \\ &0 < y_{CO_2}^{flue}, y_{H_2O}^{flue} < 0.2 \end{aligned} \tag{12}$$

The former fixes the total amount of CO_2 and water in the flue gas (since nitrogen is assumed to be 80 $mol\%$ of the flue gas), while the latter provides upper and lower bounds for the mole fractions. Equation (12) encompasses the potential carbon dioxide fraction of typical PCC power plants (Danaci et al., 2021). The lower and upper bounds for the PE problems establish a finite estimation search space and are not included in the RTO economic optimization problem as the disturbances and parameters are not decision variables in the RTO formulation.

4. Results and discussion

The formulations outlined in section 2 are implemented in the PCC system described in section 3. Measurement noise is inserted to the estimation scheme via the steady-state measurement samples $\{\boldsymbol{z_{t-i}}\}_{i=0}^{M}$ and is assumed to be additive zero-mean Gaussian noise with a standard deviation of 5% of the nominal measurement values (i.e., $\mathcal{N}(0, (0.05\boldsymbol{z_{nom}})^2)$, such that the noise can substantially affect estimate quality. $\boldsymbol{z_{nom}}$ is the measurement vector corresponding to the nominal operating conditions outlined in section 3.2.

Each scenario studied herein features different assumptions regarding uncertainty, thus various operating schemes are deployed. The sensitivity of the cost-optimal process operation is studied in Scenario A assuming no uncertainty. Scenario B features model (parametric uncertainty) only, while Scenario C jointly considers model and economic uncertainty. Accordingly, the suitable schemes in section 2.1. and section 2.2. are assessed in Scenario B and Scenario C, respectively, through their effects on a long (months) timescale according to the metrics defined in section 3. Moreover, the proposed methods are compared to alternative operating schemes, these include: our previous work (Patrón and Ricardez-Sandoval, 2022a), which omitted uncertainty; and a comparison to DR (Özyurt and Pike, 2004), which lv-PE has not been tested against previously.

4.1. Scenario A: Sensitivity of cost-optimal operation

Power plants often follow a diurnal schedule whereby the electricity produced observes a time-of-use (TOU) pricing model. TOU works such that price of energy is changed over the day so that providers can disincentivize excessive consumption through periods of peak demand.

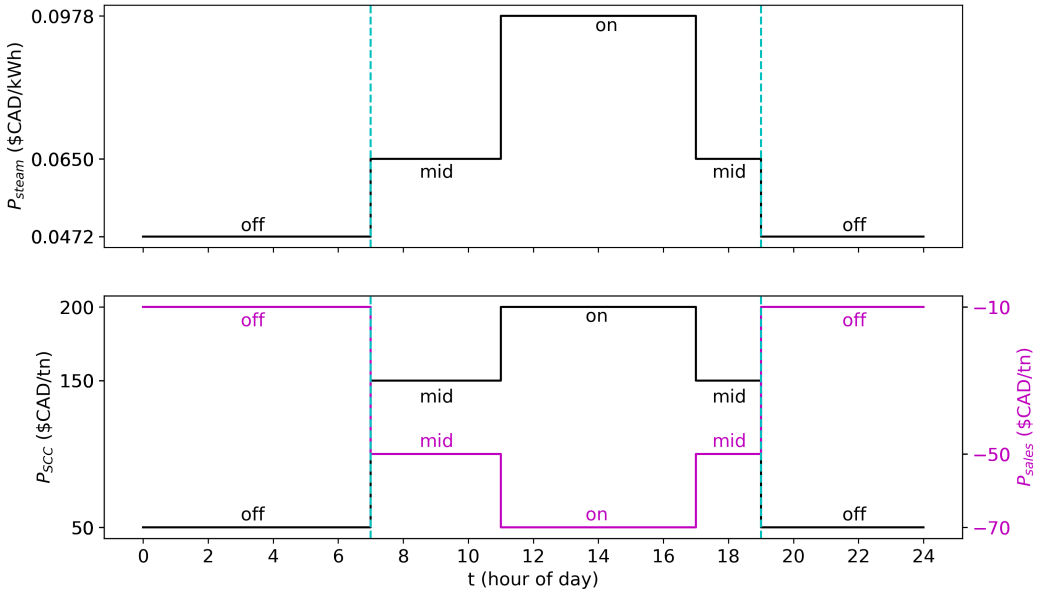

Figure 3: TOU variation in steam price (top), SCC and carbon sales (bottom). Cyan dotted lines denote update times for Scenario C.

As mentioned in section 3.1., the main cost of PCC has been found to be the energy consumption, which is manifested in steam fed to the reboiler. Accordingly, the price of steam is varied in the same TOU manner as electricity (i.e., since the steam could otherwise be used for power generation). Consumer pricing fluctuation amplitudes and timings were retrieved from the Ontario Energy Board (2021) for a 24-hour summer cycle. These amplitudes were incorporated into the steam price reported in Karimi et al. (2011). As such, electrical losses via steam consumption to the PCC plant vary in the same manner as electricity price to consumer; this is depicted in Figure 3 (top). Moreover, SCC (Nordhaus, 2017) and carbon sales rates (Nwaoha and Tontiwachwuthikul, 2019) were also assumed to vary in the same schedule and amplitude with high, medium, and low values taken from the literature (Figure 3, bottom). These are scheduled to incentivize removal during on-peak hours of high demand, with lesser incentives in off-peak hours of low demand. While current carbon economies do not consider live pricing of sales and tax rates, a future integrated carbon economy is likely to deploy these mechanisms to regulate the production of carbon. This can be done similarly to how electricity prices are set according to the TOU generation capacity (e.g., the steam price in the top pane of Figure 3).

A sensitivity analysis was performed for the cost-optimal PCC operation under variation of the disturbances of flue gas inlet flowrate (F_0^g) and flue gas CO_2 content ($y_{CO_2}^{flue}$). This is done as previous studies only consider a limited set

of disturbance realizations, which are far more limited than the ranges typically observed in the literature (e.g., Danaci et al., 2021). The flue gas flowrate is assumed to vary within a symmetric $\pm 15\%$ interval centred around its nominal value (reported in section 3), i.e., $F_0^g = \alpha \boldsymbol{d_{nom}}$ where $\alpha \in [0.85,1.15]$. Furthermore, the flue gas CO_2 content can manifest between the range $y_{CO_2}^{flue} \in [0.12,0.175]$. In addition to variation of disturbances, the prices can manifest at the three levels (off, mid, on) corresponding to TOU as depicted in Figure 3. For this scenario, the uncertain mode parameters are assumed to be perfectly known and manifesting at their nominal values as reported in section 3. Figure 4 shows the sensitivity analysis performed of the cost optimal operation.

Generally, a trend of increasing and sensitive capture rates is observed with increasing flue gas CO_2 content as evidenced in the first row of Figure 4. These increased optimal rates are coupled with a decreased process cost (second row of Figure 4) as the PCC process can operate more efficiently with a more concentrated inlet (i.e., a more concentrated flue gas has similar effect to a more concentrated solvent). In contrast, lower removal rates are coupled with lower removal costs as the flue gas flowrate increases; however, the sensitivity to this disturbance is significantly less than the sensitivity to flue gas composition. This is owed to less efficient operation as increased throughput of flue gas requires a commensurate increase in amine concentration or reboiler duty, which is economically disadvantageous. Accordingly, in situations of higher flue gas flowrates, the optimal operating policy is to settle for low removal to minimize cost. An exception to the behaviours listed above occurs for the process cost under the off-peak regime (bottom-left pane of Figure 4). Herein, it is observed that low flue gas compositions and flowrates result in lower costs and there is little sensitivity to either disturbance. This occurs due to the weak economic incentives in the low carbon and energy costs. Accordingly, the off-peak operating regime sees only small changes in optimal pricing regardless of the disturbance combination observed.

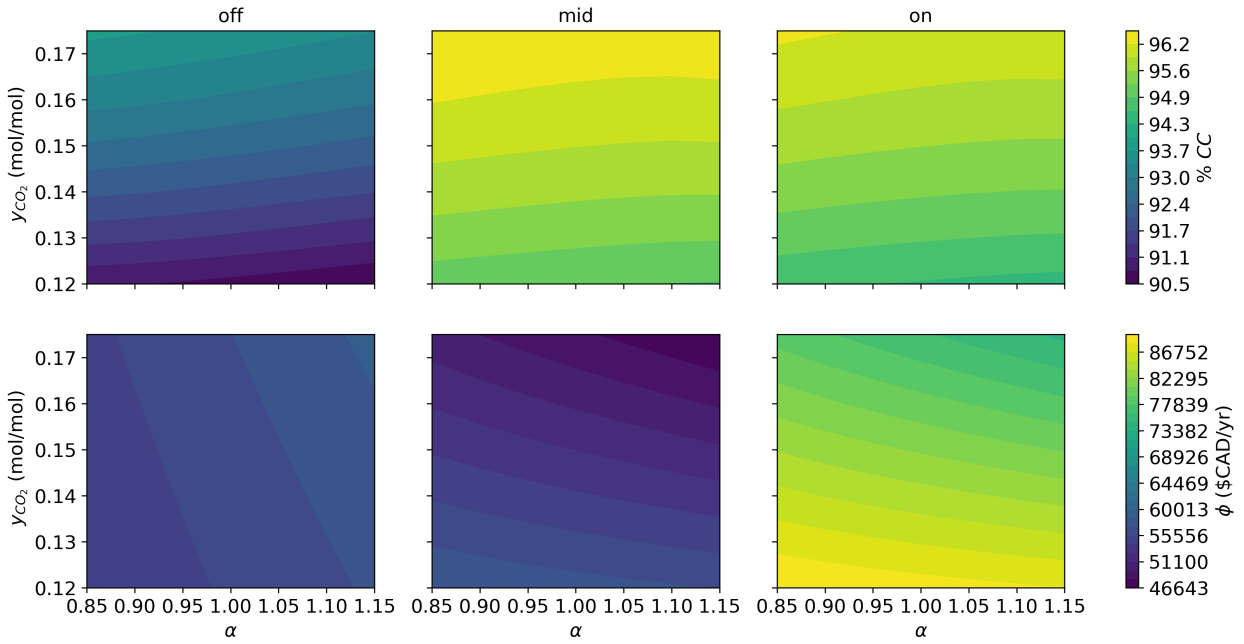

Figure 4: Cost-optimal rate of carbon capture (first row) and process cost (second row) under varying disturbances and TOU. The columns represent the TOU prices.

With respect to the TOU economic incentives, the off-peak prices result in the lowest overall capture rates with middling process costs. This occurs as the off-peak prices favour conservative operation due to low carbon costs (Figure 3); again, the off-peak prices result in decreased cost sensitivity to disturbances. This implies that the energy price dominates the operation during off-peak hours whereby low capture is favorable as there is little removal incentive and high energy detriment from excessive removal. In contrast, on-peak prices result in high capture rates with the highest costs due to the increased carbon and energy prices. In this case, reasonably high capture is achieved despite the high energy prices because the carbon prices are dominant. However, the highest removal rates and lowest prices in the TOU pricing scenarios are achieved using mid-peak incentives, which balance removal and process costs with middling carbon and energy pricing. The mid-peak incentives have unit costs that are sufficiently low to warrant high removal rates while not being low enough to drastically increase reboiling or makeup (Figure S1, Supplementary information).

The optimal price and rates of carbon capture are sensitive to both upstream disturbances and the economic incentives on the process; this is reflected in an 6.1% range in removal rates and a 43,000 $\$CAD/yr$ range in annualized process cost (see the corresponding colour bars in Figure 4). Accordingly, variation and uncertainty in these disturbances and prices will have a significant effect on the operation of PCC; thus, are suitable for parameter estimation and robust optimization in the forthcoming sections.

4.2. Scenario B: Estimation of flue gas carbon content ($\boldsymbol{\theta_d}$)

Flue gas compositions to the PCC plant may vary with respect to time as feedstock to the upstream power plant varies in grade (e.g., changes in the type of coal being used). Moreover, this variation is expected to occur in power plants that employ cofiring (Hodžić et al., 2020; Loeffler, 2014), whereby various fuel types are used within the same power unit. This necessitates an operating scheme that is flexible to different flue gas composition profiles such that the process economics are optimized despite variation.

Scenario B considers a parameter estimation approach as outlined in section 2.1., whereby the uncertain parameters are provided to the RTO and control models. To explore the effect of measurement noise on scheme effectiveness, this scenario compares four RTO implementations: 1) RTO with a standard PE and no noise-abating step (denoted PE); this represents the scheme deployed in our previous work (Patrón and Ricardez-Ssndoval, 2022a) with an additional PE layer, 2) RTO with traditional least-squares DR (Özyurt and Pike, 2004) (denoted DR-PE), 3) RTO with low-variance PE (Patrón and Ricardez-Ssndoval, 2022b) considering information content and estimation filters (denoted lv-PE), and 4) RTO with knowledge of the true value of the CO_2 content (denoted TV). The latter of these cases is unrealistic as composition measurements of the flue gas are difficult to perform online in practice; however, it provides an upper bound to economic performance as it results in an RTO model with no mismatch from the plant. The PE/RTO is run for 100 RTO periods of $\Delta T = 8\ hours$ (i.e., 33 $days$) as to have a large sample of RTO executions and sufficiently long RTO periods. The main unmeasured disturbance/estimated parameter ($\boldsymbol{\theta_d}$ as defined in section 3.2) is the flue gas CO_2 content ($y_{CO_2}^{flue}$), which is varied for each RTO period. Danaci et al. (2021) provides a breakdown of the flue gas CO_2 compositions for different fuel types/grades; based on the range reported therein, the flue gas CO_2 molar fraction was sampled from a uniform distribution between 0.12 and $0.175\ mol/mol$ (i.e., $y_{CO_2}^{flue} \sim \mathcal{U}(0.12, 0.175)$). The PE deployed in this scenario must estimate this content such that it can provide the RTO and control models with accurate information regarding the disturbance. The results from these implementations are shown in Figure 5.

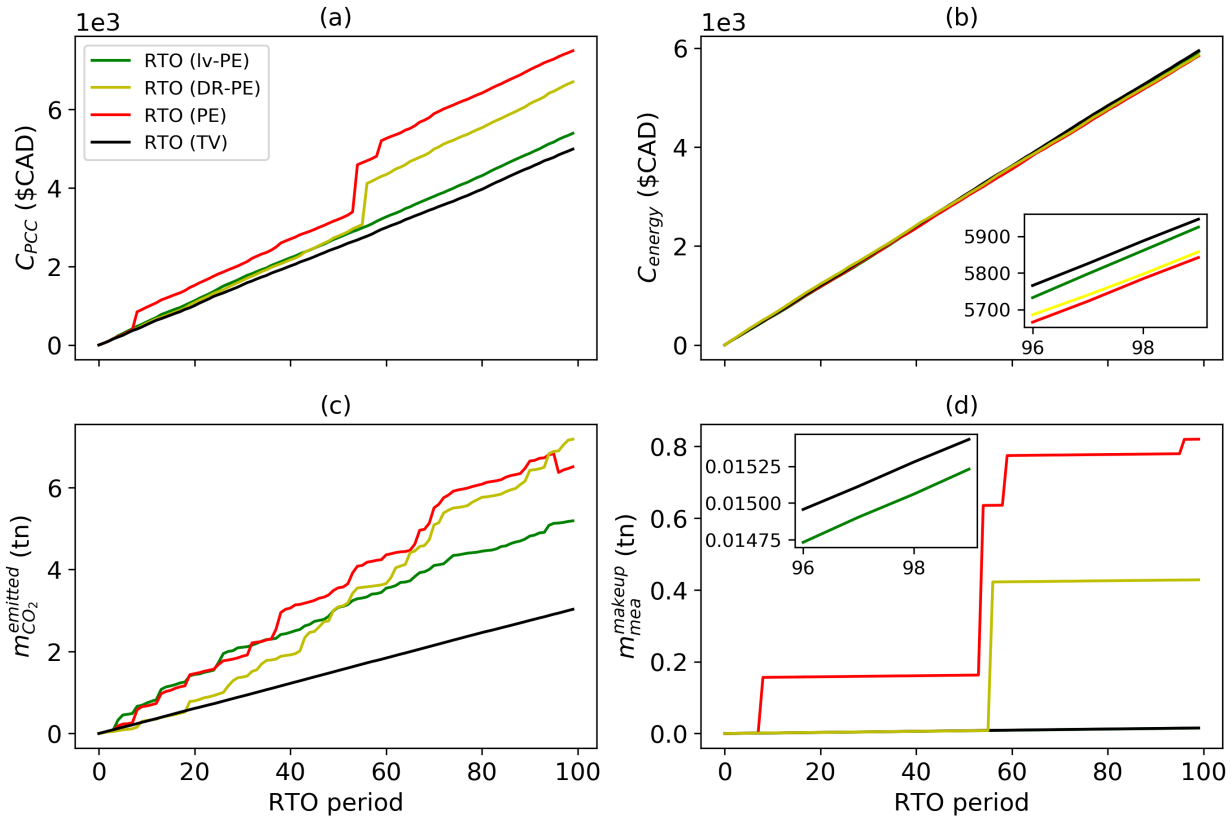

Figure 5: Cumulative a) PCC cost, b) energy penalty, c) CO_2 emissions, d) fresh MEA used for scenario B.

As illustrated in Figure 5a, the cumulative PCC cost, as defined in equation (7), over the 100 RTO periods tested is significantly more expensive for the PE and DR-PE than the lv-PE (~39% and ~25% more expensive, respectively). With respect to the TV case, the PE, DR-PE and lv-PE experience economic losses of ~50%, ~34%, and ~8%, respectively; as such, the lv-PE is the most cost-effective, followed by the DR-PE, and the PE. Comparing the benchmark DR-PE with the proposed lv-PE in Figure 5a, it can be observed that the two schemes indeed have similar performance until period 55 whereby the economic profiles diverge. This is owed to an erroneous parameter estimate, which was discarded by the lv-PE scheme by the filter bounds. In contrast, this does not occur with the DR-PE scheme, leading to an expensive period of operation. Moreover, the estimation schemes make subtle difference in abating energy penalties as in Figure 5b (in fact, the TV case and lv-PE incur a slightly higher energy penalty). This is likely the main driver of decreased emissions (i.e., increased removal) observed in Figure 5c, whereby higher reboiler duty leads to increased removal.

In contrast, as shown in Figure 5c and d respectively, the CO_2 emissions and MEA consumption can vary substantially depending on the scheme used. The emissions over the 100 RTO periods tested are ~115%, ~137%, and ~70% higher when using the PE, DR-PE, and lv-PE, respectively, over the TV case. This constitutes another improvement

of the lv-PE and a deterioration of the DR-PE with respect to the PE case. While the lv-PE performs better than the PE and DR-PE, it is worse than the measurable disturbance case. This suggests that the CO_2 emissions predictions generated by the PCC model are highly sensitive to uncertainties in flue gas composition, which is reasonable as the upstream composition will directly impact the outlet compositions. Moreover, the DE/RTO and DR-PE/RTO require a significantly higher amount of fresh MEA that the lv-PE and TV cases. Indeed, this appears to be the main factor elevating the PCC cost in the PE and DR-PE schemes as steps in the MEA consumption depicted in Figure 5d align with steps in cost depicted in Figure 5a. As mentioned above, these are likely caused by outlier parameter estimates in the PE implementation, which are filtered by the lv-PE such that an unnecessary makeup is not used. This finding also aligns with our previous work, where the MEA makeup was shown to be a major source of PCC cost. In addition to the cumulative plots, the average parameter error across the three estimation schemes tested are $\sim 30\%$, $\sim 35\%$, and $\sim 40\%$ for the lv-PE, DR-PE, and PE schemes, respectively. Notably, the limitations of our previous work are shown in the PE case, whereby its economic and emissions performance are worse under uncertainty ($\sim 42\%$ and $\sim 45\%$ additional deterioration with respect to the true parameter case, respectively).

As reported in our previous work (Patrón and Ricardez-Ssndoval, 2022a) the averaged CPU time for the RTO is 4.33 s. Additionally, the mean PE CPU time as determined in this study is 4.45 s. As such, RTO and PE models are fit for online use.

4.3. Scenario C: rRTO under diurnal economic variation and activity coefficient ($\boldsymbol{\theta_p}$) uncertainty

In this scenario, the TOU pricing model in Figure 3 was considered to formulate an update strategy for the PCC that considers prices that vary at irregular intervals. Scenario C considers the rRTO update strategy described in section 2.2. and is assessed across 100 $days$ worth of operation. The cyan vertical dotted lines in Figure 3 denote RTO update times; 12-hour periods lengths were chosen as the long and expensive transients observed in Patrón and Ricardez-Sandoval (2022a) prohibit frequent set point updating, especially in cases where prices vary quickly. The update strategy assumes the RTO is executed at the beginning of the off-peak night operation (19: 00) as shown in Figure 3, whereby the RTO can exploit the constant low overnight price. The second update occurs at the beginning of daytime (7: 00), which begins a succession of price changes to mid-peak (denoted m) and on-peak (denoted o) consumption levels. Both strategies are subject to the economic fluctuations ($\boldsymbol{P_t}$) depicted in Figure 3 as well as uncertainty in $\boldsymbol{\theta_p}$ (i.e., the thermodynamic activity coefficients as described in section 5.2.).

Three contrasting RTO schemes were compared. An RTO with knowledge of the true parameter values (labelled tRTO) was implemented and uses a "live" price (i.e., the price at the time at which the RTO is executed). The tRTO is unrealistic since the true parameter values are never known; however, it provides an upper bound for the system's performance. Moreover, a "naïve" update strategy (labelled nRTO henceforth) was also deployed, which updates the RTO set point based on the live price and updates the parameters using the two-step approach without making use of the lv estimation formulation (this is equivalent to Patrón and Ricardez-Ssndoval (2022a) with an added PE layer). Lastly, a robust strategy (labelled rRTO henceforth) updates the set point based on the expectation that the price will vary a few times in the coming 12-hour period and that the uncertain parameters manifest with a uniform distribution. Accordingly, the rRTO formulation in equation (3) is deployed with the following weights:

$$\omega_{t,k} = \frac{t_k}{\sum_{k=1}^{n_p} t_k} \times \frac{n_p}{n_r} \tag{13}$$

where t_k denotes the operating length associated with each economic scenario $k \in \{1, \dots, n_p\}$ and n_r is the total number of parameter scenarios. The operating times (t_k) weigh the scenarios in the objective function such that prices which are operated at for longer are prioritized; these timings known *a priori* as TOU timings schedules are pre-determined by the Ontario Energy Board (2021). In the daytime period where the costs vary within a short amount of time, this formulation is deployed such that a single operating point that is robust to the prices is used rather than using an operating point that is optimal for a short period of time and subsequently suboptimal. To restrict the model size when using the multi-scenario formulation, the uncertain parameters are assumed to manifest at their 95% confidence interval lower ($\boldsymbol{\theta}^{\boldsymbol{l}}_{\boldsymbol{p,t}}$) and upper ($\boldsymbol{\theta}^{\boldsymbol{h}}_{\boldsymbol{p,t}}$) bounds as defined in section 2.3. Respective scenarios used in the formulation, denoted as l and h, are shown in Table 2. These bounds are determined by the lv-PE algorithm using the parameter estimate statistics prior to the execution of the rRTO and are updated at new operating points to accommodate varying levels of uncertainty. Moreover, the uncertain economics are also assumed to manifest at the mid-peak (m) and on-peak (o) prices when performing the daytime set point update, respectively $\boldsymbol{P}^{\boldsymbol{l}}_{\boldsymbol{t}} = \boldsymbol{P}^{\boldsymbol{m}}_{\boldsymbol{t}}$ and $\boldsymbol{P}^{\boldsymbol{h}}_{\boldsymbol{t}} = \boldsymbol{P}^{\boldsymbol{o}}_{\boldsymbol{t}}$, as shown in Figure 3. Table 2 shows the economic scenarios considered in the present rRTO.

The RTO-operated system is simulated for 100 $days$ to generate costs/savings of the deployment of the rRTO with respect to the RTO; these are shown in Table 3 for clarity (plots can also be found in Figure S2, Supplementary information).

Table 2: Realization in uncertain parameters and economic function for rRTO.

Uncertainty	S1	S2	S3	S4	S5	S6	S7	S8	S9	S10	S11	S12	S13	S14	S15	S16
γ_{MEA}	h		h		h		h		l		l		l		l	
γ_{CO_2}	h		h		l		l		l		l		h		h	
γ_{H_2O}	h		l		h		l		l		h		l		h	
ϕ	m	o	m	o	m	o	m	o	m	o	m	o	m	o	m	o

Table 3: Cumulative results for Scenario C over the testing period.

Scheme	Period	C_{PCC} ($\$CAD$)	C_{energy}($\$CAD$)	$m_{CO_2}^{emitted}$ (tn)	m_{MEA}^{makeup} (kg)
rRTO	Daytime	8148.80	9056.14	4.48	25.12
	Overnight	7119.14	8286.15	7.95	21.31
nRTO	Daytime	8271.48	9108.18	4.65	23.88
	Overnight	7207.64	8393.87	7.73	21.44
tRTO	Daytime	8076.01	9006.85	4.52	24.05
	Overnight	7117.63	8629.10	7.82	21.40

As summarized in Table 3, the rRTO scheme only experiences total of ~0.48% economic performance deterioration with respect to the tRTO case whereas the nRTO deteriorates by ~1.9% over the time observed herein. The former is achieved through a ~1.7% reduction in energy penalty enabled by ~2.2% higher MEA consumption, which results in ~0.75% higher CO_2 emissions when compared to the tRTO. Distinguishing between daytime and overnight periods, the rRTO is found to only experience ~0.9% deterioration in the former and ~0.02% in the latter. When compared to the corresponding ~2.4% and ~1.3% daytime and overnight deteriorations for the nRTO, the benefit of economic robustness becomes apparent. During the daytime period when prices fluctuate, the multi-scenario economic function of the rRTO outperforms that of the nRTO and results in a larger discrepancy between the two schemes.

The economic benefits of using a robust approach are less than those when the parameter update scheme is deployed for flue gas composition as in scenario B. This suggests that the PCC process is less sensitive to the activity coefficient estimates despite them being uncertain in reality. Moreover, this is consistent with the "price of robustness", whereby a robust solution must sacrifice performance of a specific scenario for optimality in the uncertainty region. However, small improvements can result in significant savings if the process is expensive as with PCC and longer time periods allow for further accretion of economic benefit. Extrapolating to a year's worth of operation (this simulation length would be computationally prohibitive), the rRTO scheme would continue to outperform the nRTO leading to ~5% annual process cost improvement. This would result in total savings of ~2,250 $\$CAD$ over an extrapolated annual

PCC cost of a ~45,000 $\$CAD/yr$. As the PCC plant studies herein is a pilot plant, the benefits of would be even more significant in an industrial scale plant where costs are higher.

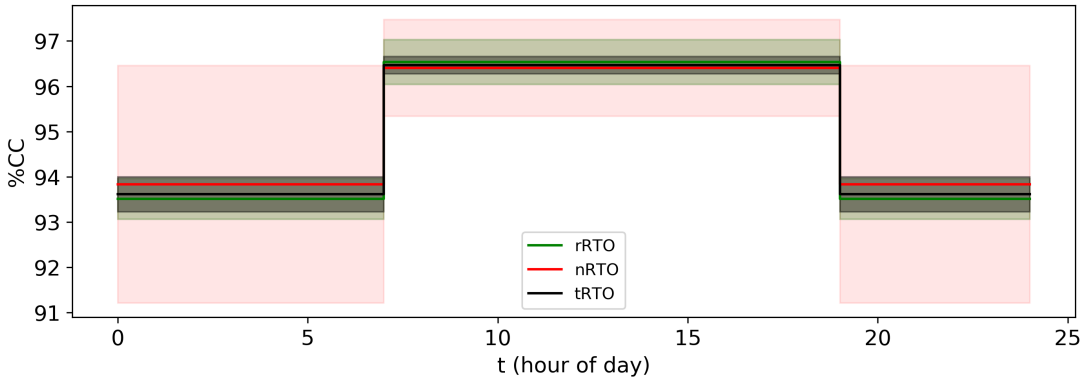

Figure 6: %CC set point trajectory statistics over 100-day testing period.

In terms of set point, the $\%CC$ set point is lower in the overnight period as shown in Figure 6. This occurs as there is less incentive for carbon removal as reflected in the low overnight SCC and sales rates in Figure 3 (bottom). In contrast, the $\%CC$ set point are significantly (~3%) higher during the daytime when the removal incentives are stronger. As the nRTO finds the daytime set point with the live $7{:}00$ prices, this under-incentivizes the removal during the daytime period where the prices increase owing to the TOU fluctuations. In contrast, the robust formulation in the rRTO takes this variation into account and chooses higher daytime removal set point to account for periods of high carbon prices, hence the higher $\%CC$ set point. Additionally, the nRTO is over-removing CO_2 in the overnight period where removal incentives are not as strong, hence a higher $\%CC$ set point; this is owed to increased error in parameter estimates when using the traditional PE approach when compared to a robust approach like the rRTO.

As the rRTO does not produce parameter estimates, the $\%CC$ is used as a proxy for operational variability. Figure 6 shows the statistics of the capture level's diurnal schedule over the testing period, with lines representing means and shaded regions representing standard deviations for each scheme considered in this scenario. As displayed therein, the daytime set points under the rRTO, nRTO, and tRTO are $96.53 \pm 0.50\%$, $96.40 \pm 1.06\%$, and $96.46 \pm 0.19\%$, respectively. Furthermore, the overnight set points under the rRTO, nRTO, and tRTO are $93.51 \pm 0.45\%$, $93.83 \pm 2.62\%$, and $93.61 \pm 0.38\%$, respectively. Accordingly, operation variability (as reflected in the standard deviations) is significantly reduced using the rRTO with respect to the nRTO. In contrast, the nRTO set points experience higher deviation than the rRTO set points despite being subject to the same disturbances and the same lv estimation scheme. As observed in the previous scenarios and in our past study (Patrón and Ricardez-Ssndoval, 2022a), reduced dynamic operation that results from reduced set point variability can impact operational costs. While the tRTO remains the

best-performing scheme in terms of economics and set point variability, the rRTO appears to show only small economic deterioration and set point variability (recall that tRTO is an idealistic scenario as discussed above). The latter is desirable from a controllability standpoint as the controller is put under less burden while maintaining relatively inexpensive process economics. Finally, the price robustness of the rRTO appears to have an effect under the quickly fluctuating daytime price profiles explored herein, which are typical in the diurnal operation of power plants. Again, the use of the lv-PE layer to provide robustness provides performance benefits with respect to the scheme provided in our previous work (Patrón and Ricardez-Ssndoval, 2022a); these are reflected in the improvement rRTO provides over nRTO with respect to cost, resource use, and emissions shown in Table 3 and Figure 6.

5. Conclusions

This work presents an RTO for PCC systems under operational and model uncertainty, which is manifested through the flue gas composition and activity coefficients, respectively. The lv-PE approach is deployed, which is designed to abate the propagation of measurement noise to parameter estimates; this is the first noise-abatement scheme deployed in the PCC literature. Furthermore, a robust RTO is used to determine an update strategy for the diurnal operation of PCC systems in cases with jointly uncertain model and economics.

The findings herein indicate that the lv-PE schemes are more successful in their estimation with respect to the traditional DR scheme and approach the true economic optima with an ~8% loss compared to a known parameter case; this is contrasted with ~34% loss for the DR scheme. Moreover, the emissions and solvent consumption of the lv estimation scheme was also found to be consistently lower than the DR/estimation scheme. The results indicate that, while estimation scheme with DR can work well, the use of lv-PE can significantly improve the system performance. Furthermore, the RTO with lv-PE can come very close to the theoretical limit (i.e., RTO with true parameter knowledge), thus resulting in nearly optimal performance observed in previous studies where uncertainties were left unaddressed. Over the period tested, the present study also found that the use of the rRTO updating strategy for periods of high price fluctuations can result in cost savings of about ~1.4% and up to ~80% set point variability reduction over the two-step approach. All case studies observe economic improvements of real-time decision-making on long timescales. With respect to our previous work (Patrón and Ricardez-Ssndoval, 2022a), the results herein indicate that a simple PE layer is insufficient to consistently provide high-quality operating points in noisy environments with fluctuating economics; this is seen through consistent improvements in cost, environmental

673 performance, and resource use. Accordingly, the proposed schemes impart the necessary robustness to deal with these
674 realistic scenarios.

675 **Acknowledgements**

676 The authors would like to acknowledge the Natural Sciences and Engineering Research Council of Canada (NSERC)
677 for their financial support.

Nomenclature

PCC process symbols		**Operational scheme symbols**	
Component concentration (mol/L)	C_i	Control horizon	C
Molar flowrate (mol/s)	F	Disturbance variables	$\boldsymbol{d}$
Liquid level (m)	h	Mechanistic model	$\boldsymbol{f}$
Mass flowrate (tn/s)	$\dot{m}$	Inequality constraints	$\boldsymbol{g}$
Component molar mass (g/mol)	M_i	Observation model	$\boldsymbol{h}$
Price of k ($\$CAD/unit$)	P_k	Covariance matrix	$\boldsymbol{K}$
Duty (W)	Q	Measurement sample size	M
Fluid temperatures (K)	T	Number of/dimension	n
Gas molar fraction (mol/mol)	y	Number of RTO periods	N
Flue gas flowrate multiplier	α	Prediction horizon	P
Column height (m)	z	Economic uncertainties	$\boldsymbol{P}$
Activity coefficient	γ	Weighting matrix	$\boldsymbol{Q}$
Efficiency factor	η	Weighting matrix	$\boldsymbol{R}$
Percent carbon capture (%)	$\%CC$	Time	t
		Manipulated variables	$\boldsymbol{u}$
PCC Subscripts and superscripts		States	$\boldsymbol{x}$
Absorber	abs	Controlled variables	$\boldsymbol{y}$
Captured by absorber	cap	Measurements	$\boldsymbol{z}$
Chemical feeds	$chem$	Controller sampling time	Δt
Buffer tank cooling	$cool$	RTO period	ΔT
Carbon dioxide	CO_2	Standard deviation	$\boldsymbol{\sigma}$
Electricity sold to consumers	$elec$	Uncertain parameters	$\boldsymbol{\theta}$
Emitted from PCC system	$emitted$	Measurement noise	$\boldsymbol{v}$
Energy penalty	$energy$	t-value	τ
Flue gas stream	$flue$	Economic function	$\boldsymbol{\phi}$
Gas	g		
Top of absorber column	H	**Operational scheme subscripts and superscripts**	
Water	H_2O	Annum/year	$annum$
Into unit	in	Controller	c
Liquid	l	Cost	C
Mid-peak	m	External uncertain model parameters	d
Makeup stream	$mkup$	Estimated quantity/estimation	e
Monoethanolamine	MEA	Finite elements in column height domain	fez
Nominal	nom	Upper bound	h
Nitrogen gas	N_2	Lower bound	l
On-peak	o	Low variance parameter estimation	$lv-PE$
Out of unit	out	Measured quantity	m
Reboiler heating	reb	Moving horizon estimation	MHE
Recycle stream	rec	Mean squared error	MSE
Captured carbon sales	$sales$	Nonlinear model predictive control	$NMPC$
Steam generated by power generation	$steam$	Internal uncertain model parameters	p
Buffer tank	$tank$	Parameter estimation	pe
Emitted from absorber in vent gas	$vent$	PCC process case study	$process$
Bottom of absorber column	0	Post-combustion capture	PCC
		Robust real-time optimization	$rRTO$
Accents		Real-time optimization	RTO
Model prediction/estimate	$\hat{}$	Steady-state	s
Average	$\bar{}$	Set point	sp
		Current time period	t

		True (i.e., not estimated) quantity	T
		Initial condition/time	0

679

References

ABB, 2003. Measurement of CO_2 in Flue Gases. SS/6515_2.

Akula. P., Eslick, J., Bhattacharyya, D., Miller, D.C., 2021. Model Development, Validation, and Optimization of an MEA-Based Post-Combustion CO_2 Capture Process Under Part Load and Variable Capture Operations. *Ind. Eng. Chem. Res.,* 60(14), 5176–93. https://doi.org/10.1021/acs.iecr.0c05035.

Artanto, Y., Jansen, J., Pearson, P., Do, T., Cottrell, A., Meuleman, E., Feron, P., 2012. Performance of MEA and amine-blends in the CSIRO PCC pilot plant at Loy Yang Power in Australia. *Fuel*, 101, 264–275. https://doi.org/10.1016/j.fuel.2012.02.023.

Bahakim, S.B., Ricardez-Sandoval, L.A., 2015. Optimal Design of a Postcombustion CO_2 Capture Pilot-Scale Plant under Process Uncertainty: A Ranking-Based Approach. *Ind. Eng. Chem. Res*., 54(15), 3879–3892. https://doi.org/10.1021/ie5048253.

Ben-Mansour, R., Habib, M.A., Bamidele, O.E., Basha, M., Qasem, N.A.A., Peedikakkal, A., Laoui, T., Ali, M., 2016. Carbon capture by physical adsorption: Materials, experimental investigations and numerical modeling and simulations – A review. *Appl. Energy,* 161, 225–255. https://doi.org/10.1016/j.apenergy.2015.10.011.

Bhat, S.A., Saraf, D.N., 2004. Steady-State Identification, Gross Error Detection, and Data Reconciliation for Industrial Process Units. *Ind. Eng. Chem. Res*., 43, 4323–4336. https://doi.org/10.1021/ie030563u.

Carminati, H.B., Milão, R.dF.D., de Medeiros, J.L., Araújo, O.dQ.F., 2019. Bioenergy and full carbon dioxide sinking in sugarcane-biorefinery with post-combustion capture and storage: Techno-economic feasibility. *Appl. Energy,* 254, 113633. https://doi.org/10.1016/j.apenergy.2019.113633.

Cerrillo-Briones, I.M., Ricardez-Sandoval, L.A., 2019. Robust optimization of a post-combustion CO_2 capture absorber under process uncertainty. *Chem. Eng. Res. Des*., 144, 386–396. https://doi.org/10.1016/j.cherd.2019.02.020.

Chan, L.L.T., Chen, J., 2018. Economic model predictive control of an absorber-stripper CO_2 capture process for improving energy cost. *IFAC-PapersOnLine,* 51(18), 109–14. https://doi.org/10.1016/j.ifacol.2018.09.284.

Chansomwong, A., Zanganeh, K.E., Shafeen, A., Douglas, P.L., Croiset, A., Ricardez-Sandoval, L.A., 2014. Dynamic modelling of a CO_2 capture and purification unit for an oxy-coal-fired power plant. *Int. J. Greenh. Gas Control,* 22, 111–122. https://doi.org/10.1016/j.ijggc.2013.12.025.

Chao, C., Deng, Y., Dewil, R., Baeyens, J., Fan, X., 2021. Post-combustion carbon capture. Renew. *Sust. Energ. Rev*., 138, 110490. https://doi.org/10.1016/j.rser.2020.110490.

Danaci, D., Bui, M., Petit, C., Mac Dowell, N., 2021. En Route to Zero Emissions for Power and Industry with Amine-Based Post-combustion Capture. *Environ. Sci. Technol.,* 55(15), 10619–10632. https://doi.org/10.1021/acs.est.0c07261.

Darby, M.L., Nikolaou, M., Jones, J., Nicholson, D., 2011. RTO: An overview and assessment of current practice. *J. Process Control,* 21(6), 874–884 https://doi.org/10.1016/j.jprocont.2011.03.009.

Decardi-Nelson, B., Liu, J., 2022. Robust Economic MPC of the Absorption Column in Post-Combustion Carbon Capture through Zone Tracking. *Energies,* 15(3), 1140. https://doi.org/10.3390/en15031140.

Decardi-Nelson, B., Liu, S., Liu, J., 2018. Improving flexibility and energy efficiency of postcombustion CO_2 capture plants using economic model predictive control. *Processes,* 6(9), 135. https://doi.org/10.3390/pr6090135.

Dugas, E., 2006. Pilot plant study of carbon dioxide capture by aqueous monoethanolamine. University of Texas at Austin; Master's thesis.

Ellis, M., Durand, H., Christofides, P.D., 2014. A tutorial review of economic model predictive control methods. *J. Process Control,* 24(8), 1156–78. https://doi.org/10.1016/j.jprocont.2014.03.010.

Gaspar, J., Ricardez-Sandoval, L., Jørgensen, J.B., Fosbøl, P.L., 2016. Controllability and flexibility analysis of CO_2 post-combustion capture using piperazine and MEA. *Int. J. Greenh. Gas Control,* 51, 276–289. https://doi.org/10.1016/j.ijggc.2016.06.003.

Hart, W.E., Watson, J.P., Woodruff, D.L., 2011. Pyomo: modeling and solving mathematical programs in Python. *Math. Program. Comput.* 3, 219–260. https://doi.org/10.1007/s12532-011-0026-8.

Harun, N., Nittaya, T., Douglas, P.L., Croiset, E., Ricardez-Sandoval, L.A., 2012. Dynamic simulation of MEA absorption process for CO_2 capture from power plants. *Int. J. Greenh. Gas. Control,* 10, 295–309. https://doi.org/10.1016/j.ijggc.2012.06.017.

Hodžić, N., Kazagić, A., Smajević, I., 2016. Influence of multiple air staging and reburning on NOx emissions during co-firing of low rank brown coal with woody biomass and natural gas. *Appl. Energy,* 168, 38–47. https://doi.org/10.1016/j.apenergy.2016.01.081.

Huang, B., Xu, S., Gao, S., Liu, L., Tao, J., Niu, H., Ming, C., Jian, C., 2010. Industrial test and techno-economic analysis of CO_2 capture in Huaneng Beijing coal-fired power station. *Appl Energy,* 87(11), 3347–3354. https://doi.org/10.1016/j.apenergy.2010.03.007.

Hughes, R., Kotamreddy, G., Bhattacharyya, D., Omell, B., Matuszewski, M., 2022. Modeling and Bayesian Uncertainty Quantification of a Membrane-Assisted Chilled Ammonia Process for CO_2 Capture. *Ind. Eng. Chem. Res.*, 61(11), 4001–4016. https://doi.org/10.1021/acs.iecr.1c04601.

International Energy Agency (IEA), 2021. Global Energy Review 2021. IEA 2021. [Online] https://www.iea.org/reports/global-energy-review-2021.

Jiang, Y., Mathias, P.M., Freeman, C.J., Swisher, J.A., Zheng, R.F., Whyatt, G.A., Heldebrant, D.J., 2021. Techno-economic comparison of various process configurations for post-combustion carbon capture using a single-component water-lean solvent. *Int. J. Greenh. Gas Control,* 106, 103279. https://doi.org/10.1016/j.ijggc.2021.103279.

Jung, H., Im, D., Heo, S., Lee, J.H., 2020. Dynamic analysis and linear model predictive control for operational flexibility of post-combustion CO_2 capture processes. *Comput. Chem. Eng.,* 140, 106968. https://doi.org/10.1016/j.compchemeng.2020.106968.

Kaewsichan, L., Al-Bofersen, O., Yesavage, V.F., Selim, M.S., 2001. Predictions of the solubility of acid gases in monoethanolamine (MEA) and methyldiethanolamine (MDEA) solutions using the electrolyte-UNIQUAC model. *Fluid Phase Equilib.,* 183–184, 159–171. https://doi.org/10.1016/S0378-3812(01)00429-0.

Karimi, M., Hillestad, M., Svendsen, H., 2011. Capital costs and energy considerations of different alternative stripper configurations for post combustion CO_2 capture. *Chem. Eng. Res. Des.,* 89(8), 1229–1236. https://doi.org/10.1016/j.cherd.2011.03.005.

Khalilpour, R., Mumford, K., Zhai, H., Abbas, A., Stevens, G., Rubin, E.S., 2015. Membrane-based carbon capture from flue gas: a review. *J. Clean. Prod*. 103, 286–300. https://doi.org/10.1016/j.jclepro.2014.10.050.

Liu, H., Idem, R., Tontiwachwuthikul, P., 2019. *Post-combustion CO2 Capture Technology By Using the Amine Based Solvents*. Springer, Switzerland. https://doi.org/10.1007/978-3-030-00922-9.

Loeffler, D., Anderson, N., 2014. Emissions tradeoffs associated with cofiring forest biomass with coal: A case study in Colorado, USA. *Appl. Energy,* 113, 67–77. https://doi.org/10.1016/j.apenergy.2013.07.011.

Lucio, M., Ricardez-Sandoval, L.A., 2020. Dynamic modelling and optimal control strategies for chemical-looping combustion in an industrial-scale packed bed reactor. *Fuel,* 262, 116544. https://doi.org/10.1016/j.fuel.2019.116544.

Luu, M.T., Abdul Manaf, N., Abbas, A., 2015. Dynamic modelling and control strategies for flexible operation of amine-based post-combustion CO_2 capture systems. *Int. J. Greenh. Gas. Control,* 39, 377–89. https://doi.org/10.1016/j.ijggc.2015.05.007.

763 Ma, K., Shi, T., Hu, Y., Yang, S., Shen, W., He, C., Liu, Y., Liu, Z., Ren, J., 2022. Poultry litter utilization for waste-
764 to-wealth: Valorization process simulation and comparative analysis based on thermodynamic and techno-economic
765 assessment. *Energy Convers. Manag*., 269, 116135. https://doi.org/10.1016/j.enconman.2022.116135.
766 Mac Dowell, N., Shah, N., 2013. Identification of the cost-optimal degree of CO_2 capture: An optimisation study using
767 dynamic process models. *Int. J. Greenh. Gas Control,* 13, 44–58. https://doi.org/10.1016/j.ijggc.2012.11.029.
768 Masson-Delmotte, V. et al., 2021. Summary for Policymakers. In: Climate Change 2021: The Physical Science Basis.
769 Contribution of Working Group I to the Sixth Assessment Report of the Intergovernmental Panel on Climate Change.
770 IPCC 2021. [Online] https://www.ipcc.ch/report/ar6/wg1/#SPM.
771 Mechleri, E., Lawal, A., Ramos, A., Davison, J., Mac Dowell, N., 2017. Process control strategies for flexible
772 operation of post-combustion CO_2 capture plants. *Int. J. Greenh. Gas. Control,* 57, 14–25.
773 https://doi.org/10.1016/j.ijggc.2016.12.017.
774 Miletic, I.P., Marlin, T.E., 1998. On-line Statistical Results Analysis in Real-Time Operations Optimization. *Ind.*
775 *Eng. Chem. Res*., 37(9), 3670–3684. https://doi.org/10.1021/ie9707376.
776 Monañés, R.M., Flø, N.E., Nord, L.O., 2018. Experimental results of transient testing at the amine plant at Technology
777 Centre Mongstad: Open-loop responses and performance of decentralized control structures for load changes. *Int. J.*
778 *Greenh. Gas Control,* 73, 42–59. https://doi.org/10.1016/j.ijggc.2018.04.001.
779 Nordhaus, W., 2017. Revisiting the social cost of carbon. *Proc. Nat. Acad. Sci. U.S.A*. 114(7), 1518–1523.
780 https://doi.org/10.1073/pnas.1609244114.
781 Nwaoha, C., Tontiwachwuthikul, P., 2019. Carbon dioxide capture from pulp mill using 2-amino-2-methyl-1-propanol
782 and monoethanolamine blend: Techno-economic assessment of advanced process configuration. *Appl. Energy,* 250,
783 1202–1216. https://doi.org/10.1016/j.apenergy.2019.05.097.
784 Ontario Energy Board (OEB), 2021. Electricity rates, https://www.oeb.ca/rates-and-your-bill/electricity-rates; 2021
785 [accessed 31 August 2021].
786 Özyurt, D.B., Pike, R.W., 2004. Theory and practice of simultaneous data reconciliation and gross error detection for
787 chemical processes. *Comput. Chem. Eng.,* 28(3), 381–402. https://doi.org/10.1016/j.compchemeng.2003.07.001.
788 Panahi, S., Skogestad, S., 2012. Economically efficient operation of CO_2 capturing process. Part II. Design of control
789 layer. *Chem. Eng. Process.,* 52, 112–24. https://doi.org/10.1016/j.cep.2011.11.004.

Patrón, G.D., Ricardez-Sandoval, L., 2020a. Real-Time Optimization and Nonlinear Model Predictive Control for a Post-Combustion Carbon Capture Absorber. *IFAC-PapersOnLine,* 53(2), 11595–11600. https://doi.org/10.1016/j.ifacol.2020.12.639.

Patron, G.D., Ricardez-Sandoval, L., 2020b. A robust nonlinear model predictive controller for a post-combustion CO_2 capture absorber unit. *Fuel,* 265, 116932. https://doi.org/10.1016/j.fuel.2019.116932.

Patrón, G.D., Ricardez-Sandoval, L., 2022a. An integrated real-time optimization, control, and estimation scheme for post-combustion CO_2 capture. *Appl. Energy,* 308, 118302. https://doi.org/10.1016/j.apenergy.2021.118302.

Patrón, G.D., Ricardez-Sandoval, L., 2022b. Low-Variance Parameter Estimation Approach for Real-Time Optimization of Noisy Process Systems. *Ind. Eng. Chem. Res*., 61(45), 16780–16798. https://doi.org/10.1021/acs.iecr.2c02897.

Rúa, J., Hillestad, M., Nord, L.O., 2021. Model predictive control for combined cycles integrated with CO2 capture plants. *Comput. Chem. Eng.,* 146, 107217. https://doi.org/10.1016/j.compchemeng.2020.107217.

Shi, T., Liu, Y., Yang, A., Sun, S., Shen, W., Ren, J., 2022. Developing a novel gasification-based sludge-to-methanol utilization process and exergy-economic-environmental (3E) analysis. *Energy Convers. Manag*., 260, 115600. https://doi.org/10.1016/j.enconman.2022.115600.

Straathof, A., Bampouli, A., 2017. Potential of commodity chemicals to become bio-based according to maximum yields and petrochemical prices. *Biofuels Bioprod. Biorefining,* 11(5), 798–810. https://doi.org/10.1002/bbb.1786.

Tontiwachwuthikul, P., Wilson, M., Idem, R., 2022. CO_2-capture research and Clean Energy Technologies Research Institute (CETRI) of University of Regina, Canada: history, current status and future development. *Clean Energy,* 6(1), 119–126. https://doi.org/10.1093/ce/zkab056.

Wächter, A., Biegler, L.T., 2005. On the implementation of an interior-point filter line-search algorithm for large-scale nonlinear programming. *Math. Program.,* 106, 25–57. https://doi.org/10.1007/s10107-004-0559-y.

Wu, Q., Lin, Q.G., Wang, X.Z., Zhai, M.Y., 2015. An inexact optimization model for planning regional carbon capture, transportation and storage systems under uncertainty. *Int. J. Greenh. Gas. Control,* 42, 615–628. https://doi.org/10.1016/j.ijggc.2015.09.017.

Xu, D., Li, W., Ren, X., Shen, W., Dong, L., 2020. Technology selection for sustainable hydrogen production: A multi-criteria assessment framework under uncertainties based on the combined weights and interval best-worst projection method. *Int. J. Hydrog. Energy*, 45(59), 34396–34411. https://doi.org/10.1016/j.ijhydene.2019.09.030.

Xuan, A., Shen, X., Guo, Q., Sun, H., 2022. Two-stage Planning for Electricity-Gas Coupled Integrated Energy System with Carbon Capture, Utilization, and Storage Considering Carbon Tax and Price Uncertainties. *IEEE Trans. Power Appar. Syst.,* 1–13. 10.1109/TPWRS.2022.3189273.

Yin, X., Decardi-Nelson, B., Liu, J., 2020. Distributed monitoring of the absorption column of a post-combustion CO_2 capture plant. *Int. J. Adapt. Control Signal Process.,* 34(6), 757–776. https://doi.org/10.1002/acs.3074.

Yuan, Y., Khatibisepehr, S., Huang, B., Li, Z., 2015. Bayesian Method for Simultaneous Gross Error Detection and Data Reconciliation. *AIChe J.,* 68(3), 3232–3248. https://doi.org/10.1002/aic.14864.

Zantye, M.S., Arora, A., Faruque Hasan, M.M., 2019. Operational power plant scheduling with flexible carbon capture: A multistage stochastic optimization approach. *Comput. Chem. Eng.,* 130, 106544. https://doi.org/10.1016/j.compchemeng.2019.106544.

Zhang, Q., Turton, R., Bhattacharyya, D., 2018. Nonlinear model predictive control and H_∞ robust control for a post-combustion CO_2 capture process. *Int. J. Greenh. Gas Control,* 70, 105–116. https://doi.org/10.1016/j.ijggc.2018.01.015.

Zhang, S., Zhuang, Y., Liu, L., Zhang, L., Du, J., 2019. Risk management optimization framework for the optimal deployment of carbon capture and storage system under uncertainty. *Renew. Sust. Energ. Rev.,* 113, 109280. https://doi.org/10.1016/j.rser.2019.109280.

Zhang, X., Zhang, X., Liu, H., Li, W., Xiao, M., Gao, H., Liang, Z., 2017. Reduction of energy requirement of CO2 desorption from a rich CO2-loaded MEA solution by using solid acid catalysts. *Appl. Energy,* 202, 673–684 https://doi.org/10.1016/j.apenergy.2017.05.135.